Employing Preprocessor Filters to Suppress the Effect of Impulsive Noise on Communications Systems at Millimeter-Wave Frequencies

Lara Mohammad Hamza Shhab

Submitted to the
Institute of Graduate Studies and Research
in partial fulfillment of the requirements for the degree of

Doctor of Philosophy
in
Electrical and Electronic Engineering

Eastern Mediterranean University
July 2020
Gazimağusa, North Cyprus

Approval of the Institute of Graduate Studies and Research

Prof. Dr. Ali Hakan Ulusoy
Director

I certify that this thesis satisfies all the requirements as a thesis for the degree of Doctor of Philosophy in Electrical and Electronic Engineering.

Assoc. Prof. Dr. Rasime Uyguroğlu
Chair, Department of Electrical and Electronic Engineering

We certify that we have read this thesis and that in our opinion it is fully adequate in scope and quality as a thesis for the degree of Doctor of Philosophy in Electrical and Electronic Engineering.

Prof. Dr. Ali Hakan Ulusoy
Co-Supervisor

Prof. Dr. Ahmet Rizaner
Supervisor

Examining Committee

1. Prof. Dr. Hasan Amca
2. Prof. Dr. Ergun Erçelebi
3. Prof. Dr. Aykut Hocanın
4. Prof. Dr. İsmail Kaya
5. Prof. Dr. Ahmet Rizaner

ABSTRACT

With the explosive growth of mobile traffic demand, the contradiction between capacity requirements and spectrum shortage becomes increasingly prominent. The bottleneck of wireless bandwidth becomes a key problem of the Fifth Generation (5G) wireless networks that could offer high level of reliability, low levels of latency and constant connectivity anytime, anywhere.

As one of its most promising potential technologies, Millimeter wave (mmWave) communication endorses 5G goals through the utilization of 30 gigahertz (GHz)-300 GHz frequency band. The high frequencies of mmWave technology allocate more bandwidth to provide multi-gigabit communication services and reinforce their applicability in cellular communications and radar alongside employing high gain steerable antennas.

However, using such frequencies and multi antennas may offer signal attenuation, blockage through obstacles, besides a noise behavior. Noise over mmWave system can be any sort of undesired fluctuation, nevertheless, the catastrophic presence of Impulsive Noise (IN) at high frequencies band whether it is a man-made noise, electromagnetic interference, non-Gaussian clutter, or nonstationary chaos, will shed the light on how much it affects the mmWave system.

In this thesis, we examine IN impact on mmWave system and suppressing its effect through implementing clipping, blanking and hybrid preprocessors. Hybrid gains the lowest bit error rate over clipping and blanking in variant impulsive environments and at different Signal to Noise Ratio (SNR) values. At several impulsive cases, the

optimal threshold values were obtained for all filters by proposing a new thresholding mechanism to eliminate IN components and maximize SNR performance. Blanking has the potential to become the preferred filter in achieving better spectral efficiency than clipping for mmWave system at different SNR and probability of IN occurrence values. The thesis shows that the use of clipping, blanking and hybrid filters with the optimal threshold values reduces the unfavorable effect of IN and improves system performance significantly.

Keywords: fifth generation, millimeter wave, impulsive noise, clipping, blanking, hybrid.

ÖZ

Mobil trafik talebinin olağanüstü büyümesiyle, kapasite gereklilikleri ve spektrum yetersizliği arasındaki çelişki giderek daha belirgin hale gelmektedir. Bu kapsamda kablosuz bant genişliğinin darboğazı, her zaman ve her yerde yüksek güvenilirlik, düşük gecikme seviyesi ve sürekli bağlantı sağlayabilen Beşinci Nesil (5G) kablosuz ağların önemli sorunları olarak kabul edilmektedir.

Gelecek neslin potansiyeli yüksek teknolojilerinden biri olarak kabul edilen Milimetre Dalga (mmWave) iletişimi, frekans bandının 30 gigahertz (GHz) ile 300 GHz arasında kullanılmasıyla 5G hedeflerini desteklemektedir. Yüksek frekanslı mmWave teknolojisi, çoklu gigabit iletişim hizmetleri sağlamak ve hücresel iletişim, radar ve büyük miktarda veri iletimi için uygulanabilirliğini güçlendirmek için daha fazla bant genişliğinin tahsis edilmesini kolaylaştırmaktadır.

Bununla birlikte, bu gibi yüksek frekansların ve çok antenli sistemlerin kullanılması, genel olarak iletişim kanalının güvenilirliğini etkileyebilecek ve performansını bozabilecek bir gürültü davranışının yanı sıra, ciddi bir sinyal zayıflaması, engellerin üzerinden tıkanma yaratabilmektedir. MmWave sistemi üzerindeki gürültü, herhangi bir tür istenmeyen dalgalanma olabileceği gibi, insan yapımı bir gürültü, elektromanyetik girişim, Gauss olmayan dağınıklık veya durağan olmayan bir kaos olup olmadığına bakılmaksızın, yüksek frekanslar bandında Anlık Gürültü (IN)'nün yıkıcı etkisinin mmWave sistemini ne kadar etkilediğine ışık tutabilmektedir.

Bu tezde, IN'in mmWave sistemi üzerindeki etkisine ve kırpma, sıfırlama ve hibrit ön filtrelerinin kullanılmasının mmWave üzerindeki etkisi incelenmektedir. Hibrit,

değişken anlık gürültü ortamlarında ve farklı Sinyal-Gürültü Oranı (SNR) değerlerinde kırpma ve sıfırlama filtresine göre daha düşük bir bit hata oranı vermektedir. Çeşitli anlık gürültü durumlarında, IN bileşenlerini ortadan kaldırmak ve SNR performansını en üst düzeye çıkarmak için yeni bir eşik mekanizması önerilerek tüm filtreler için optimum eşik değerleri elde edilmiştir. Sıfırlama, farklı SNR ve anlık gürültü olasılık değerlerinde mmWave sistemi için kırpmadan daha iyi spektral verimlilik elde etmiş olup tercih edilen filtre olma potansiyeline sahiptir. Tez, kırpma, sıfırlama ve hibrit filtrelerinin en uygun eşik değerleriyle kullanılması neticesinde IN'in olumsuz etkilerini azalttığını ve sistem performansını önemli ölçüde geliştirdiğini göstermektedir.

Anahtar Kelimeler: beşinci nesil, milimetre dalgası, anlık gürültü, kırpma, sıfırlama, hibrit.

DEDICATION

This dissertation is dedicated to:

My Father, and My Mother,

Your unlimited endorsement and endless encouragement enlighten my life.

ACKNOWLEDGMENT

My above all gratitude goes to the Almighty God for granting me the fortitude, power, and forbearance to finish my doctoral journey.

I would like to express my sincere gratitude to my precious supervisors Professor Ahmet Rizaner and Professor Ali Hakan Ulusoy for their great support, valuable guidance, and never-ending encouragement throughout my study. Also, I would like to express my tremendous appreciation to Professor Hasan Amca for his priceless support and insightful opinions. My dear professors, your kindness and patience made my study more enjoyable and informative.

My beloved family, your endless love, encouragement and eternal patience highly stimulated my strength and determination. I owe to you with everlasting thanks and favors.

I am indebted to all my valuable friends who supported me over the past years; you have made my educational experience so delightful and memorable. In particular, my beloved friend Faegheh.

I would also like to extend my thanks to everyone who kept caring and asked about the end of this journey.

TABLE OF CONTENTS

LIST OF TABLES

LIST OF FIGURES

LIST OF SYMBOLS AND ABBREVIATIONS

16-QAM	Sixteen symbols-Quadrature Amplitude Modulation
1G	First Generation
2G	Second Generation
2-QAM	Two symbols-Quadrature Amplitude Modulation
3G	Third Generation
4G	Fourth Generation
4-QAM	Four symbols-Quadrature Amplitude Modulation
5G	Fifth Generation
A^+	Peak amplitude of impulsive noise burst
A	Impulse index
A	Business area man made noise
a_0	First filter coefficient of optimal threshold polynomial
a_1	Second filter coefficient of optimal threshold polynomial
a_2	Third filter coefficient of optimal threshold polynomial
a_3	Fourth filter coefficient of optimal threshold polynomial
a_4	Fifth filter coefficient of optimal threshold polynomial
a_5	Sixth filter coefficient of optimal threshold polynomial
$\mathbf{a}_{\mathrm{BS}}$	Normalized transmit response vector
AM	Amplitude Modulation
$\mathbf{a}_{\mathrm{MS}}$	Normalized received response vector
AoA	Angle of Arrival
AWGN	Additive White Gaussian Noise

AWGGN	Additive White Generalized Gaussian Noise
B	Galactic noise
BER	Bit Error Rate
BS	Base Station
C	Galactic noise with infinite narrow beam
CE	Channel Estimation
c_i	Weight coefficient vector
D	Quiet sun noise
DAC	Digital to Analog Converter
DOA	Directional of Arrivals
E	Sky noise with 0^o and 90^o elevation angles
$e^{-j\varphi_r}$	Phase argument for clipping/blanking filters
F	Cosmic noise
f	Total noise power density function of mixture distribution
$f(x)$	Overall noise density function for ε-mixture model
F_a	External noise figure
$f_b(x)$	Noise density function for Gaussian background noise
$\mathbf{F}_{\mathrm{BB}}$	Baseband precoder matrix
$f_G(x, \mu_i, \sigma_i^2)$	Gaussian power density function
$f_{GM}(x)$	Power density function of Gaussian mixture model with *k* components
FMCW	Frequency-Modulated Continuous-Wave
$f_o(x)$	Noise density function for impulsive noise
$f_{P+G}(x)$	Power density function of class A noise
$\mathbf{F}_{\mathrm{RF}}$	Radio frequency precoder matrix
$\mathbf{F}_{\mathrm{T}}$	Base station precoding matrix

GHz	Giga Hertz
GPS	Global Positioning System
GSM	Global System for Mobile Communication
H	Millimeter wave channel matrix
H_2O	Water vapor
HPBW	Half Power Beam Width
IN	Impulsive Noise
k	Number of signal samples
K	Proportionality constant
L	Number of paths of the channel
$L_{free\ space}$	Free space loss for a movable millimeter wave
LOS	Line of Sight
LNA	Low Noise Amplifier
LTE	Long Term Evolution
m	Impulsive sequence
M	Number of symbols for quadrature amplitude modulation
MAC	Media Access Control
MIMO	Multi Input Multi Output
ML	Maximum Likelihood
mmWave	millimeter Wave
MS	Mobile Station
n	Overall noise corrupting the received signal
$N(.)$	Gaussian probability density function
$N(0, \sigma_w^2)$	Gaussian power density function of mixture distribution
$N(0, \sigma_z^2)$	Impulsive power density function of mixture distribution

N_{BS}	Number of antennas in base station
$n_i(m)$	Amplitude modulated binary state sequence
NLOS	Non Line of Sight
N_{MS}	Number of antennas in mobile station
N_{RF}	Number of radio frequency chains
N_{S}	Number of data streams
O_2	Oxygen
OFDMA	Orthogonal Frequency Division Multiple Access
p	Ration between Gaussian background noise and impulsive noise
P_{av}	Average received power
pdf	Power density function
PLC	Power Line Communications
PS	Phase Shifters
PSD	Power Spectral Density
QAM	Quadrature Amplitude Modulation
$\|\mathbf{r}\|$	Norm of vector **r**
$\mathbf{r}$	Received signal vector
R	Mutual information rate of spectral efficiency
R_a	Separating distance between transmitter and receiver
$\mathbf{r}_{\mathrm{b}}$	Output vector of blanking filter
$r_{\mathrm{b}}(i)$	Output vector for blanking filter
$\mathbf{r}_{\mathrm{c}}$	Output vector of clipping filter
$r_{\mathrm{c}}(i)$	Output vector for clipping filter
$\mathbf{r}_{\mathrm{f}}$	Filtered received signal
$\mathbf{r}_{\mathrm{h}}$	Output vector of hybrid filter

$r_{\mathrm{h}}(i)$	Output vector of hybrid filter
RF	Radio Frequency
$r(i)$	Input vector for clipping/blanking filters
$\lvert r(i)\rvert$	Absolute value of the i^{th} component of the vector **r**
r_k	Output of the nonlinear filter
$r_{\mathrm{N}}(i)$	Normalized received signal vector
s	Transmitted symbol vector
SαS	Symmetric Alpha Stable
SINR	Signal to Impulsive Noise Ratio
SNR	Signal to Noise Ratio
SNRE	Effective Signal to Noise Ratio
T_1	Clipping threshold
T_2	Blanking threshold
t_{arr}	Arrival time of impulsive noise burst
T_b	Blanking threshold
T_{bo}	Optimal threshold for blanking filter
T_c	Clipping threshold
T_{co}	Optimal threshold of clipping filter
t_{l-arr}	Inter-arrival time between successive bursts
$T_{\mathrm{o}}(\gamma_e, \epsilon)$	Optimal threshold polynomial
t_w	Width of impulsive noise burst
$u_k(\theta_k, t)$	k^{th} interferer
UMTS	Universal Mobile Telecommunication System
UPA	Uniform Planar Array
VSB	Vestigial Side Band

$\mathbf{w}$	Complex Additive White Gaussian Noise vector
$\mathbf{W}_{BB}$	Based-band combiner matrix
$\mathbf{W}_{RF}$	Radio frequency combiner matrix
$\mathbf{W}_{T}$	Mobile station combiner matrix
$\mathbf{x}$	Discrete-time transmitted signal vector
$x(t)$	Instant amplitude probability density function
$\mathbf{y}_{f}$	Output processed received signal at mobile station
y_k	Input of nonlinear filter
$\mathbf{z}$	Complex impulsive noise
α	Stability factor
α_l	Complex gain of the l^{th} path
γ	Expansion of heavy tailed impulsive noise distribution around its center
γ_e	Effective signal to noise ratio parameter
ε	Mixture parameter for the occurrence of impulsive noise
ϵ	Probability of impulsive noise occurrence
θ	Set of random variables characterizing the interference
θ_l	l^{th} path's angels of arrival
λ	Wavelength
μ_i	Mean of impulsive noise in Gaussian mixture model
ρ	Average path-loss between base station and mobile station
σ_b^2	Variance of Gaussian background noise in ε-mixture model
σ_e	Overall variance
σ_i^2	Variance of impulsive noise in Gaussian mixture model

σ_m^2	Overall variance of background noise and impulsive noise
σ_o^2	Variance of impulsive noise in ε-mixture model
σ_{w}^2	Gaussian noise variance of mixture distribution
σ_{z}^2	Impulsive noise variance of mixture distribution
ϕ_l	l^{th} path's angels of departure
$\phi_x(w)$	Characteristic function of Middleton class B model
φ_r	Phase for the nonlinear filter

Chapter 1

INTRODUCTION

The innovative depiction for the radio's capability to contact the ships continually while sailing in the English Channel was accomplished by Marconi in 1897. And since then, wireless communications have become the essence of attention all over the world as the most rapidly growing aspect of communication industry [1, 2].

The indigence for wireless emerged to match the massive requests for higher ranks of intelligence in knowledge and information in various sectors of the society. The enormous expansion in mobile traffic and volume requirements is attributed by the imperious demand for wireless connectivity, and the rising usage of mobile multimedia services.

The wireless radio systems started its temporal gradation with the First Generation (1G) utilizing the analog technology, followed by the Global System for Mobile Communication (GSM); the prevailing standard for the Second Generation (2G). Subsequently, the dawn of the Third Generation (3G) emerged with the Universal Mobile Telecommunication System (UMTS).

The phase of the next generation was identified by releasing the technical specifications of the Long Term Evolution (LTE). Based on the Orthogonal Frequency Division Multiple Access (OFDMA), LTE had the capability to give the

Fourth Generation (4G) a considerable distinction over the previous generations. The evolution of LTE provided the technology demands with higher spectrum efficiency and data rates, besides low-cost devices. By the end of 2015, LTE captured around 12% of the total market and is expected to reach above 40% by 2021. Nevertheless, LTE was not possible to meet with the evolution requirements since many new technologies and advanced technical solutions had arisen over the years following the initiation of 4G [3, 4].

Correspondingly, LTE was eligible to prop the future mobile communication through an ambitious generation. Stemming from conceiving the wide range of use cases and new radio access technology, the Fifth Generation (5G) has been founded [5, 6]. 5G expands far beyond its previous generations over a wide spectrum of applications and services exemplifying the forthcoming mobile technology. Its splendid potential drove into a global assent on commercialization around 2020 with adoption by 2025. The foresight of 5G will comprise humans and machines access to services and information regardless the time, place and the identity of the performer. It seeks into attaining the outmost-reaching integration not only the conventional wireless architectures but also the interior structure of the mobile network and its layers [3, 4, 6].

Under the market demands, 5G era will offer a platform of multi-gigabits per second and a superb refinement in cell capacity and network energy consumption. Moreover, it will accommodate the highly increasing mobility requests through excessing user data rates [5, 7]. The concept of 5G will embed the usage of the higher frequency bands which have not been employed by the previous generations. The propagation properties for those bands make them an unprecedented solution to promote and

improve the goals of 5G, as well recently, they spurred considerable attention in exploiting the large blocks of such frequencies in intensive deployments. Attributing to wavelength, the unexploited spectrum of such bands is often named as millimeter Waves (mmWaves) [4, 7].

As one of the most promising major paradigms to realize the vision of 5G, mmWaves dominate the electromagnetic spectrum within the range of 30 GHz up to 300 GHz. Stepping into this range of frequencies yields a massive increment in system capacity and bandwidth and enables mmWaves to be advantageous for a variety of implementations. Extensively, mmWaves are leveraged in plenty of indoor and outdoor applications, backhaul links, medical imaging, highly accurate multimedia streams, dynamic automation, and radar sensing. Additionally, their frequencies have elevated the level of advancements in semiconductor technology, solidity of transceivers, topology reformalization and power mitigation [6, 8-10].

The small wavelengths of mmWave frequencies aid the synthesis of many highly-gain steerable antennas at base and mobile stations. The high degree of steerability associated with spatial multiplexing for such antennas raises spectral efficiency and enables mmWave technology to exhibit the conceivable convergence of cellular and WiFi services for wireless communication and low-price Complementary Metal Oxide Semiconductor technology [11, 12].

However, mmWave technology incorporates impairments as well. While its propagation properties support the solidification of a robust high intense packed links and wireless personal area networks, on the other hand, they actuate mmWave signals to inevitable transmission losses in the air and rigid substances and frustrate

their navigation through long distances. mmWave technology might attenuate because of rain and atmosphere as absorption mediums, also it is sensitive to blockage, multipath fading, Doppler shift, and noise [6, 13].

Over the years, many studies investigated the effect of specific types of noise on the mmWave system, for instance, phase noise, measurement noise, and Gaussian noise. Nevertheless, the impact of Impulsive Noise (IN) on mmWave has not been examined or conducted.

1.1 Research Objectives

Addressing the presence of IN and detecting its impact on mmWave technology system is the main aim of this thesis. IN is modeled as a term component of the Gaussian Mixture model, while the other term component is the Gaussian noise which exemplifies the background noise in the system. Through many techniques and schemes utilized in combating IN, the nonlinear preprocessors are picked due to their simplicity and efficiency, specifically, clipping, blanking and hybrid filters.

The mechanism of clipping, blanking and hybrid filters in this thesis relies on proposing algorithms for the best IN reduction performance in a mmWave system. Furthermore, a method for estimating the optimum thresholds for clipping and blanking filters is developed in order to select the most convenient threshold in the suppression process.

1.2 Thesis Organization

The present research is perhaps the first step in contributing to a more systematic approach and is encompassed by six chapters. Tracking the main introduction is in Chapter 1. mmWave system is presented in Chapter 2 with an overlook on its characteristics and drawbacks. In addition, this Chapter focuses on the types of

mmWave channels and mmWave massive Multiple Input Multiple Output (MIMO) system with its different approaches including antenna array, precoding and channel estimation. Chapter 3 displays the definition of the IN, its characteristics and the noise modelling scheme. Further, it discusses the effect of different types of noise on mmWave system and the possibility of IN existence in such a system. Chapter 4 exhibits the nonlinear preprocessors models and the purpose of their exploitation, besides the way they operate to mitigate IN. Chapter 4 also introduces a novel algorithm based on specific thresholds for clipping, blanking and hybrid filters in order to overcome the IN presence. Chapter 5 reveals simulation results through the application of clipping, blanking and hybrid filters in a noise-contaminated environment in mmWave system to detect and diminish the IN effect. Further, it illustrates the functionality of the system through optimizing the non-linear preprocessors thresholds for the best mitigated impulsive impact result. Finally, Chapter 6 provides the key results with conclusion and presents some future works regarding the proposed field.

Chapter 2

MILLIMETER WAVE SYSTEMS

Over more than 100 years ago, Jagadish Bose laid the first mmWave communication system using spark transmitter, coherer, dielectric lens, polarizer, horn antenna and cylindrical diffraction grating. mmWave communication system was merely restricted at that time to some niche purposes correlating with radar, military and astronomical implementations [14, 15].

The extremely high frequencies dovetail with mmWaves and resided between the infrared and microwave divisions within the electromagnetic spectrum. As one of the most distinguished key elements for 5G network, mmWave is a prosperous candidate to visualize more remarkable progresses in the telecommunication space [16, 17].

2.1 Millimeter Waves Characteristics

The possession of such excessive high frequencies within the electromagnetic spectrum enables mmWave to have some distinct characteristics when compared to other segments of the spectrum [26]. The importance of mmWave characteristics is deduced through the foresight of the features and motion of any of their own representative fragment; they can be concised as [18]:

2.1.1 Narrow Beamwidth

Bearing in mind the small wavelengths, the antennas functioning at mmWaves can provide narrow beamwidths embodying less scattering and improved information gained about the nature of particular objects [19, 20].

2.1.2 Huge Bandwidth

In the entire range of 1 GHz up to 300 GHz, there is a massive unoccupied portion of bandwidth that reinforces mmWave frequency band to approve high data rates, high jam-immune systems and the reduction of multipath and interference. Greater bandwidth means more information to be transmitted, better resolution and enhanced sensitivity [20, 21].

2.1.3 Propagation Characteristics

They stand for the ways of alteration and interaction with atmosphere while they convey through. Unquestionably, they endow mmWave system a useful applications platform encompassing radar, highly-secured technology and transmitting massive data magnitudes, further, they assist mmWave frequency bands to be beneficial for backhaul links, indoor, short range, and Line of Sight (LOS) communications. However, sometimes, they restrict the ability of mmWave to contend against some technologies. Moreover, the electromagnetic energy in mmWave frequencies is exposed to interactions with atmospheric constituents greater than its counterpart in the microwave frequencies. Apart from the aforementioned, the relevant propagation characteristics comprise the following aspects [17, 20, 22].

2.1.3.1 Free Space Loss

Based on the spherical scattering for a propagating radio wave, the power attained by a receiver decays as frequency increases causing a high loss for a movable mmWave in the free space. This can be illustrated by:

$$L_{free\ space} = \left(\frac{4\pi R_a}{\lambda}\right)^2 \tag{2.1}$$

where R_a is LOS range, which is the separating distance between transmitter and receiver, λ is the wavelength [17].

2.1.3.2 Propagation Loss Factors

2.1.3.2.1 Blockage and Diffraction

The propagation through hurdles with larger dimensions than the wavelengths of electromagnetic waves obstructs their diffraction, as stated by the electromagnetic theorem. Therefore, the range of signals at mmWave frequencies is reduced since they barely penetrate through rigid objects and buildings. That's what makes them extremely impressed by the impact of blockage, diffraction and reflection, meanwhile, this is also reinforces Non Light of Sight (NLOS) communication [22, 23].

2.1.3.2.2 Atmospheric Gaseous Attenuation

When mmWaves convey through the atmosphere, they are absorbed by the ambience's gaseous components, mainly, oxygen (O_2) and water vapor (H_2O). The absorption by O_2 and H_2O molecules cause attenuation, reaching its peaks at 24 and 60 GHz. However, mmWave signals can easily propagate through some transmission windows at 35, 94, 140 and 220 GHz. Figure 2.1 depicts the relation between the atmospheric absorption and frequency for a height at sea level and 4 km [17, 24].

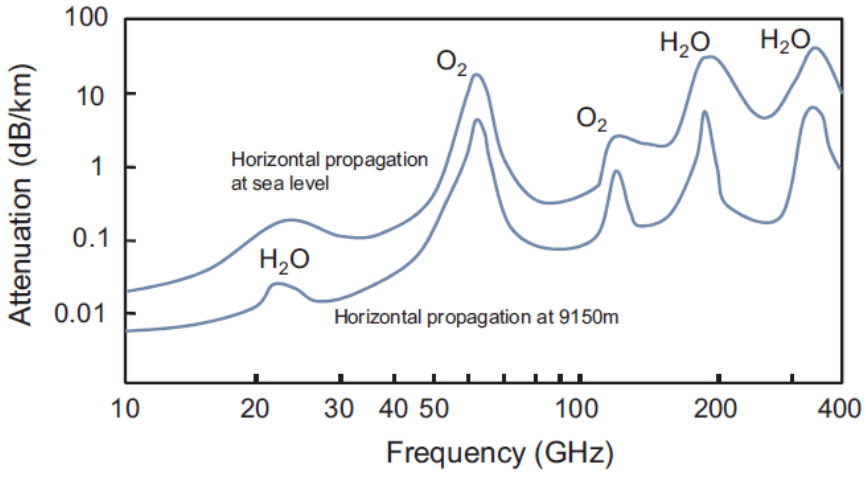

Figure 2.1: Average atmospheric absorption of mmWaves [25]

2.1.3.2.3 Rain Attenuation

Due to the consistency of the basic dimensions for both mmWaves' wavelengths and rain drops, mmWaves are exposed to a considerable attenuation while propagating through an intense rain region. Figure 2.2 illustrates the attenuation of rain at mmWave frequencies [24].

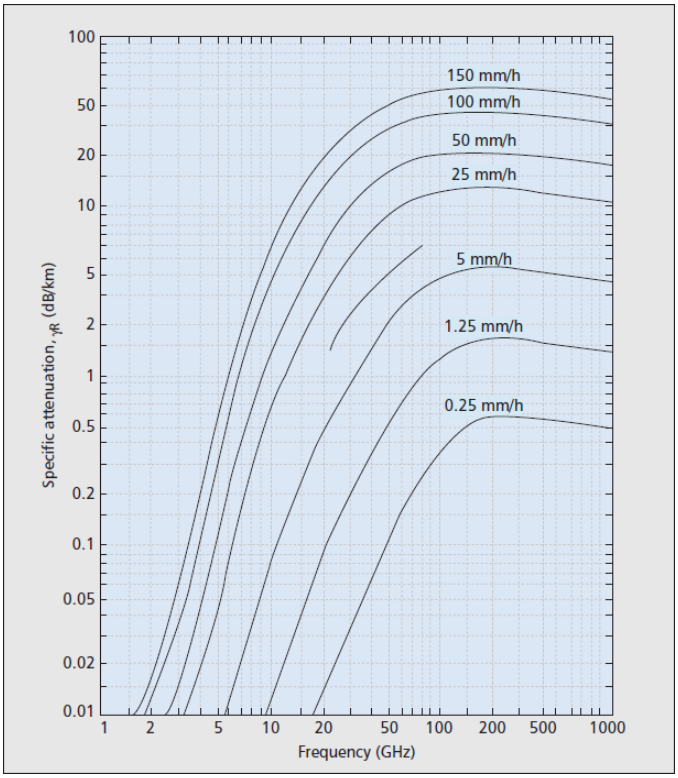

Figure 2.2: Rain attenuation at mmWave frequencies [26]

2.1.3.2.4 Sky Noise

Sky noise or brightness temperature is emitted out from the atmospheric elements and gathered by the earth station antenna. It reaches its ultimate level at the resonance bands of mmWaves altering their convenience for communication implementations [24].

In spite of the disturbing effects for the above-mentioned characteristics, somehow they might be beneficial for mmWaves in several aspects. Namely, the path loss could be theoretically compensated because of the small wavelengths of mmWaves that boost antenna gain throughout equipping a massive number of antenna elements in the same area. As well as, whilst the oxygen absorption reaches its maximum level at 60 GHz than at 30-60 GHz, however, this empowers the 60 GHz to embrace high data rates and establish an impenetrable indoor communication [20, 22].

2.2 Millimeter Waves Channel Models

Evolving the models of mmWave channel is the fundamental stride to perceive its correlated propagation characteristics in any frequency band. One of the model classifications which is structured based on the electromagnetic properties of the signal conveying between the transmitter and receiver is the physical approach and it comprises [27]:

2.2.1 Deterministic Model

It exemplifies the real impact of environment on the regime, however with extremely sophisticated computations. When there are no measurements for a particular framework, the deterministic scheme can be beneficial in anticipating the new environment features and this will minimize the operation cost. Its most convenient mechanism is the ray tracing.

2.2.2 Stochastic Model

It envisions the space and time characteristics of the channel as a probabilistic model, its channel can be considered as random since it is exposed to many entities and unknown variables. Stochastic model is easy to implement with lower complicated computations and has several approaches as Saleh Valenzuela, the 3^{rd} Generation Partnership Project, spatial channel model and Zwick model [27, 28].

2.3 The Advantages of Millimeter Waves Technology

Due to the small wavelength of mmWave, it would be possible to employ a large number of antenna elements in a spatially restricted area; this is known as the massive MIMO technique. Massive MIMO is essential for mmWave cellular communications to overcome the high propagation attenuation of mmWave technology and its low radiation power stemmed out of the small antenna size. Harnessing the high-directivity antenna can ensure that a high received power adequate for signal detection. Furthermore, mmWave system demands to operate steerable directional antennas to support multiple mobile users at variant positions instead of using the high gain dish antennas.

Exploiting a Radio Frequency (RF) front end and digital baseband for each antenna in the massive mmWave array provides an entire capacity and flexibility; however, it will be of a high cost. Further, such a fully digital mmWave massive array is also not sensible because of the narrow space limitations. Antenna elements in an array must be packed denser to avoid grating lobes. For reducing signal attenuation and interference, the analog components like the Low Noise Amplifier (LNA) (or power amplifier), frequency converter, and local oscillator should be condensed behind the antenna elements. This limited space creates a major hurdle in implementing antenna arrays at mmWave frequencies.

The hurdle can be overcome through the hybrid antenna array in which antenna elements are grouped into analog subarrays. Each phase shifter is devoted to a single antenna element and the other components are associated with antenna elements in a subarray. Any individual analog subarray accepts only one digital signal, and then

the output signals from analog subarrays would be handled together in a digital processor. Besides prevailing over space limitation challenge, such a structure can minimize the cost and complexity with fewer amounts of hardware elements.

Regarding the multipath sparsity feature of mmWave propagation channels, the hybrid array structure reinforces the strong potential for fulfilling both array diversity and multiplexing gain. NLOS component in mmWave system has much lower power compared to LOS component resulted from the fact that mmWave propagation for the multipath signal is sparse temporally and spatially. A few numbers of the multipath signals reach their targets in concentrated directions. Therefore, the analog subarray is utilizing the analog beamforming to verify a large array gain alongside with individual digital processing chains for each subarray to support multiplexing and interference cancellation.

Analog beamforming is easier to be implemented. However, analog beamforming usually suffers from serious performance loss, since only the phases of the transmit signals can be controlled. More importantly, analog beamforming is usually employed by single-user single-stream systems and the extension to multiuser multistream systems does not seem straightforward.

Employing the digital precoding is usually attaining a satisfying performance because of its capability to control both the phases and amplitudes of signals. However, it leverages the energy consumption and hardware cost through the dedication of one individual RF chain for each antenna, which makes it impractical for mmWave massive MIMO systems with a large number of antennas.

Hybrid beamforming overcomes the main drawbacks of both digital and analog beamforming. it may obtain the performance achieved by digital precoding but with a fewer number of RF chains, which can be expressed in terms of the number of data streams instead of the number of antennas. Thus, hybrid precoding appears to be more applicable for future mmWave massive MIMO systems [22].

The antenna radiation pattern for mmWave system is subjected to a rapid transition between the lower and higher frequencies in cellular systems. Therefore, for compensating the dissipated gains, applying more directive antennas at both Base Station (BS) and Mobile Station (MS) should be considered. However, to combat the inefficacy of using the individual beams, the beamformer is magnified with a multiplexed number of data streams. Hence, the distinct beams in different paths may overlap with each other that are leading to Signal to Noise Ratio (SNR) deterioration in various directions. Besides, the exposure to blockage, misalignment of beams and beamsteering passivity in a mmWave system might cause a kind of incorporation of noise and interference represented by severe rapid variations with an “On/Off” behavior [22, 29].

2.4 Millimeter Waves Massive MIMO

mmWave is regarded as one of the two technological streams in 5G technology that fulfill the demanding needs to raise data rates, bandwidths and data throughput, while the other is the multi-antenna MIMO denoting Multi Input Multi Output transceivers. MIMO outperforms the conventional single antenna system in implementing the spatial dimension to enhance the capacity and reliability. When it is applied at mmWave frequencies, MIMO manifests its flexibility by rendering the following crucial capabilities [30]:

- Beamforming gain to lift power adequacy.
- Higher spatial multiplexing to boost spectral efficiency.
- Narrower beam to improve spatial reuse.

Furthermore, MIMO system has diverse prerequisites at mmWave band compared to those in the microwave band. For example, the space-time coding MIMO scheme could foster the consistency, particularly in NLOS platform through equipping the system with diversity gains. While the space-division multiplexing which is exploited to prop MIMO capacity and raise the transmission rate is expensive and constrained with the limited bandwidth in the low frequencies band. However, in the enormous bandwidth of mmWave band, its significance is loosened [26].

As the carrier frequency increases, the number of disseminated antennas escalates to gradually aggregate a large number to be piled into a compact area at mmWave frequencies, and this is referred to as massive MIMO. Essentially, massive MIMO is eligible to promote 5G requirements without any additional bandwidth and power dissipation. Employing any of MIMO techniques on mmWave system is not restricted, nevertheless, the negative impacts of mmWave propagation characteristics should be taken into consideration [22, 26].

2.4.1 Millimeter Waves Massive MIMO System Model

mmWave massive MIMO stems its significance when mmWave and MIMO systems collaborating to combat the coexisted deficiencies in each system separately, and is manifested through the utilization of the following techniques:

2.4.1.1 Antenna Array

It is a radiating structure that comprises more than one antenna element, regardless of the way of employing the antenna elements in array formation, and how they should

be spaced in between. This gives the freedom in constructing antenna arrays with different properties that contain different elements, feeding sorting, and various separating distances between elements. Antenna arrays reinforce the capability to build the radiation patterns of beamwidth and orientation, both of which can be monitored electronically. Some antenna array types are linear, circular, conformal, and planar arrays. However, the most common one is the Uniform Linear Array (ULA) which is composed of antenna elements packed on a straight line and equally spaced by a particular distance. Each antenna element has its power represented by Half Power Beam Width (HPBW), amplitude, and phase of its feeding current which can be modified to adapt the radiated power whether being transmitted to or received from a given spatial direction. The phase of the feeding current is raised by the number of array elements proportionally, which is distinguishing ULA as a progressive phase shift array. The number of array elements is inversely proportional to the amplitudes of feeding currents and the HPBW radiated power. Intuitively, ULA is utilized to reduce HPBW by increasing the number of array elements and steering the main lobe into the intended direction by altering the progressive phase shifts. The constructed phase shifts imply the arrival angles of a signal arriving at each of the array elements, meanwhile, the resulted steering angles in the phase arrays vary with frequency [31].

2.4.1.1.1 Estimating Angle of Arrival

Angle of Arrival (AoA) stands for the direction of arrival in which a temporal waveform incident on ULA elements. To gauge AoA for a hybrid array, many chronicle trials should be executed between the digital and analog components. The way of measuring a single AoA value is embedded in the utilization of the constant phase difference between corresponding elements in two adjacent subarrays in ULA.

The low-precision estimation of AoA leads to a low-analog beamforming gain and SNR at the digital branches. AoA can be measured with respect to the normal to array aperture and is adjusted for the sake of array steering. Beam steering is a need for generating larger antenna gains at higher frequencies at both BS and MS. In mmWave systems, beam steerable antenna is employed to estimate AoA and improving shifting between different beam patterns to diminish interference and to capture the targeted signal [10, 22, 32].

2.4.1.2 Precoding (Beamforming) Schemes

Improving the throughput of mmWave massive MIMO system is accomplished by exploiting beamforming, spatial multiplexing or a synthesis of both. While the gains produced through spatial multiplexing compensate the path loss and mitigate power consumption, beamforming dominates the phases and amplitudes of transmitted signals based upon the environment and proposed technique. Precoding can be as analog, digital or hybrid [33].

2.4.1.2.1 Analog Precoding

It is conceived through a network of Phase Shifters (PS) together with a small number of RF chains. In spite of its easiness in implementation, it experiences severe performance losses due to amplitude restrictions provoked by RF chains. Figure 2.3 shows the architecture of analog beamforming for a single user where BS exploits several transmitting antennas with only one RF chain for sending one data stream to a user in MS with several receiving antennas and one RF chain [22].

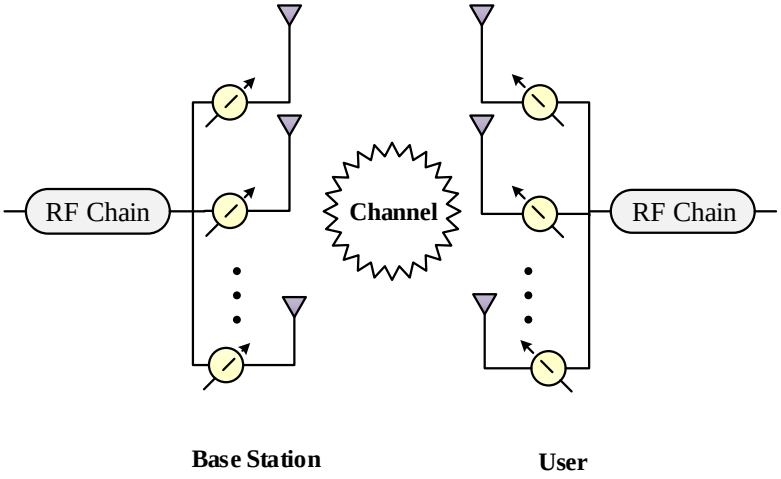

Figure 2.3: Architecture of analog beamforming for single user mmWave massive MIMO

2.4.1.2.2 Digital Precoding

It eliminates the interference through disciplining both amplitudes and phases of propagating signals, hence provides a favorable performance. Nonetheless, the devotion of one RF chain for each antenna will waste energy and leverage the hardware cost. Figure 2.4 displays the single user digital precoding scheme where BS harnesses multi transmitting antennas for sending simultaneous data streams to a user with multi receiving antennas in MS. On the other hand, the multi user digital precoding scheme is illustrated by Figure 2.5 in which BS is equipped with multi transmitting antennas and RF chains to interact concurrently with a number of MS, each individual MS is provided with multi receiving antennas [22].

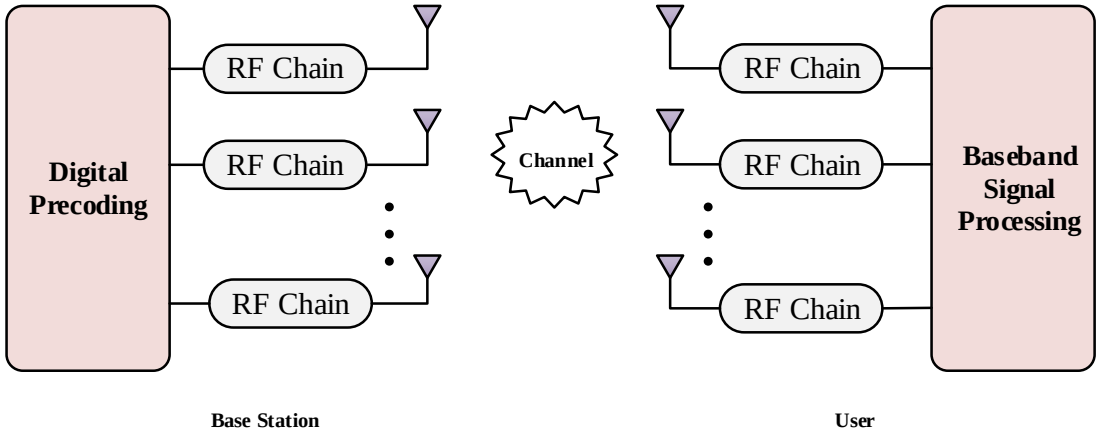

Figure 2.4: Digital precoding for single user mmWave massive MIMO

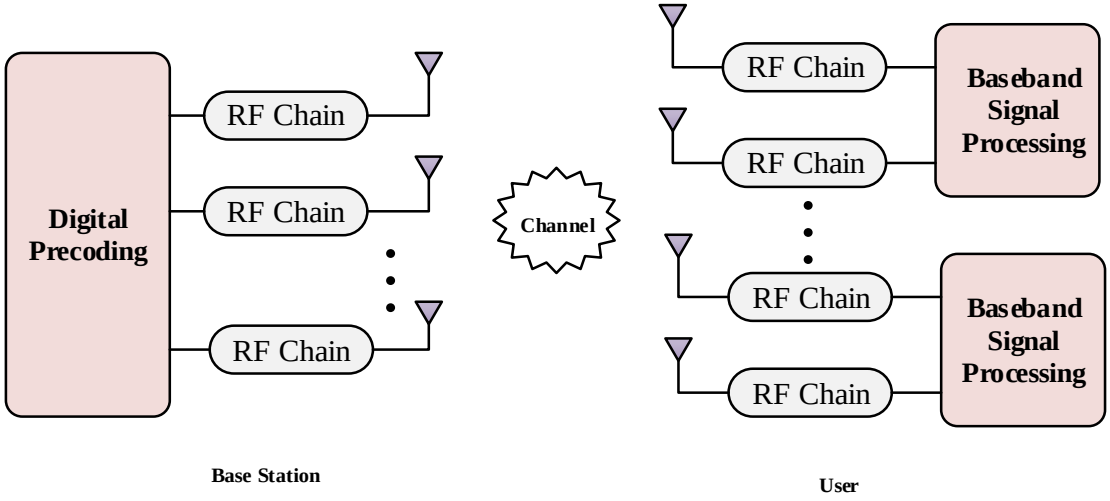

Figure 2.5: Digital precoding for multi user mmWave massive MIMO

2.4.1.2.3 Hybrid Precoding

To tackle the drawbacks of analog and digital precoding, hybrid precoding is nominated through introducing the small size digital precoder to omit the noise, then, a large size analog beamformer to raise the gain. It is working also for the single user and multi-user architectures. Where in the single user architecture illustrated by Figure 2.6, BS employs multi transmitting antennas for sending concurrent data streams to a user in MS with multi receiving antennas. However, the multistream

transmission is confirmed when BS uses digital precoder through its RF chains, followed by an analog beamformer which is utilized through PS analog circuitry.

While in the multi user architecture depicted in Figure 2.7, RF chain in BS comprises Digital to Analog Converter (DAC) and mixer filter to lower the power dissipation and lessen the losses in the chain. In order to handle many users, the system is further supplied with a group of Uniform Planar Array (UPA) antennas quantized by MN where M depicts the number of horizon antennas and N denotes the number of vertical antennas [22, 33, 34].

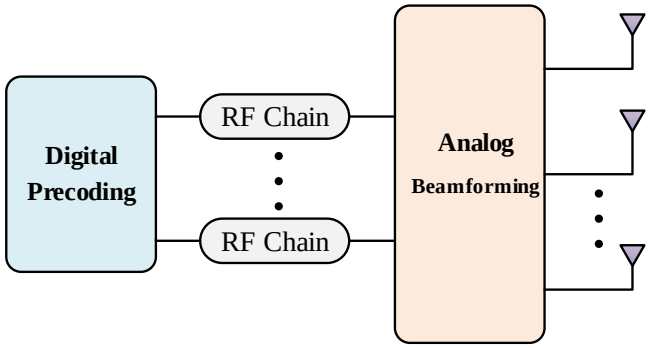

Figure 2.6: Hybrid precoding for single user mmWave massive MIMO

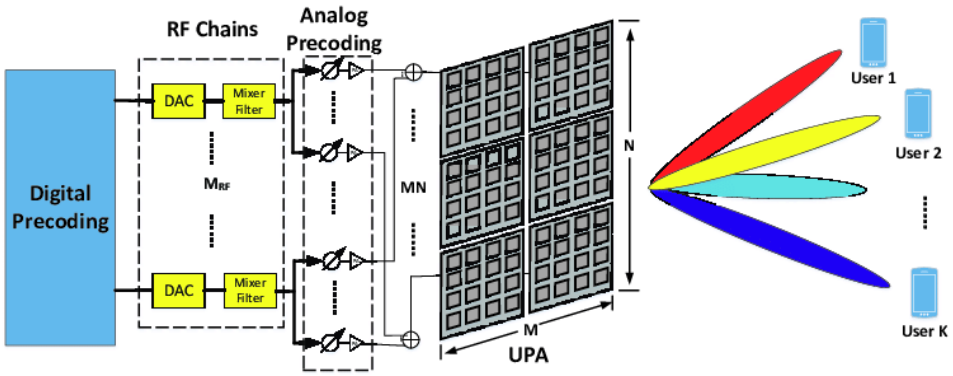

Figure 2.7: Hybrid precoding for multi user mmWave massive MIMO [34]

Further, hybrid precoding is categorized into two single user paradigms. In the fully connected paradigm, each RF chain in BS is linked to all transmitting antennas via PS since the analog beamformer is exploited through the analog PS besides harnessing LNA to attain the best SNR as shown in Figure 2.8. While the subconnected architecture outperforms the fully connected architecture in reducing the number of required PSs which can preserve energy and afford a simplified hardware scheme. As exhibited by Figure 2.9, each RF chain is linked to only a subsidiary of transmitting antennas via a set of PS along with a set of LNA [22, 33].

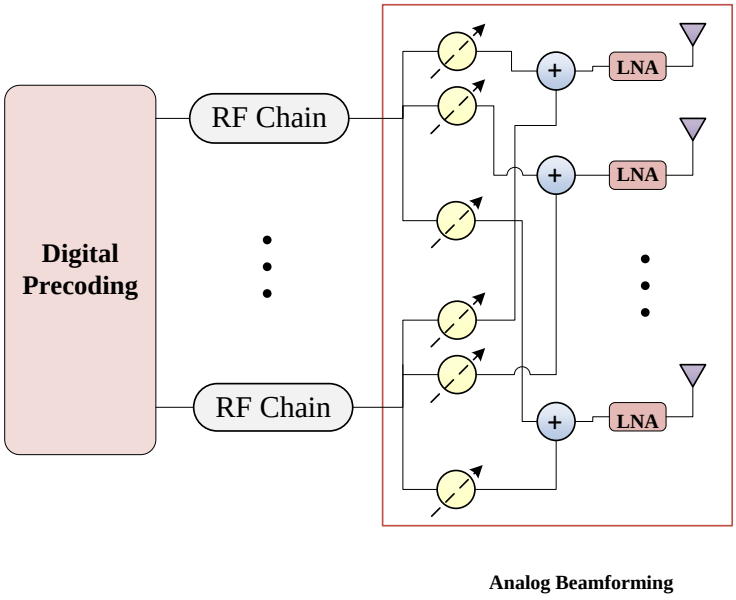

Figure 2.8: Fully connected architecture of hybrid precoding for single user mmWave massive MIMO

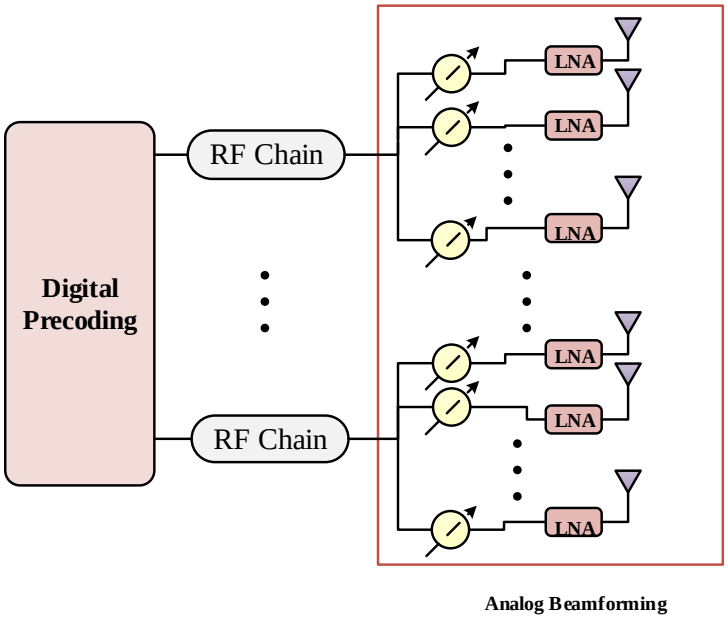

Figure 2.9: Subconnected architecture of hybrid precoding for single user mmWave massive MIMO

2.4.1.3 Channel Estimation

The layout for precoding algorithms relies on the fully channel state information, however it is hard to obtain due to the enormous number of antennas and the low SNR before beamforming, and unfortunately, the trouble is aggravated by hardware restrictions. Thus, the genuine Channel Estimation (CE) is an arduous burden and the detection of the most reliable CE scheme should conceive the followings [22, 35]:

- Signal processing in the digital baseband.
- The attributes of analog phase shifter networks.
- Doppler shift.
- Blockage effect.
- The channel reciprocity caused by time division duplex-based communication systems.
- Synchronization.
- Calibration error of RF chains.

Chapter 3

NOISE IMPACT ON MILLIMETER WAVE SYSTEMS

Any undesired perturbation that overlaps with another signal perception and transmission is usually pinpointed as noise. Noise is characterized by an information bearing nature which exemplifies knowledge about its sources and propagation in the originating environment [36]. Noise has been existed since the early incipience of electrical communications, however until 1940s; it was recognized extensively due to the emergence of probabilistic systems and Shannon mathematical communication theory. Noise is present mostly in all mediums and whether created within the telecommunication system or caused by a source outside the telecommunication system [37].

Whatever its provenance, noise contaminates transmission process and limits its capacity, besides, it restricts the radio link functionality and causes SNR degradation. Hence, noise processing and elimination have been the substantial theme of the notion and implementation of both communication system and signal processing [36, 38].

Despite the tremendous advantages for exploiting mmWave frequencies, however, the maturization submitted by such frequencies for cellular networks confronts significant technical barriers. Besides the negative impacts of mmWaves'

propagation characteristics, mmWaves are exposed to the drastic effects of interference and noise [39, 40].

3.1 Noises Effect on Millimeter Wave Systems

3.1.1 Phase Noise

It refers to the short random variations in the frequency (or phase) of an oscillator signal. Phase noise causes deterioration in both the bit error rate and the selectivity of a receiver through the addition of position shifts of constellation points and the diversion of contiguous channel energy into the desired signal's spectrum. Consequently, when phase noise exists in mmWave networks, the implementation of the multicarrier modulation systems would be a challenge [41, 42].

3.1.2 Measurement Noise

To find the strongest beam pair in the analog beamforming in mmWave systems, the received powers for a bunch of pairs are computed and discriminated within a beam training process. The process is considered a vital key for applying beam prejudice in any analog beamforming paradigm. Nevertheless, beam training cannot recognize the strongest beam when SNR is not adequately high resulting an imprecise beam alignment. Such misalignment produces measurement noise which decays power loss probability and average rate in mmWave systems [43].

3.1.3 Sky Noise

Not only atmospheric components are sources of propagation attenuation for mmWave frequencies, but also, they can radiate signals identical to noise. The radiated sky noise or brightness temperature can be gathered by any earth station antenna driven to a satellite at a high elevation angle. Whilst, the presiding noise at low elevation angles will be mostly from terrain and would be gathered by the antenna sidelobes. The impact of sky noise reaches its maximum at the mmWave

gaseous molecule resonance bands, and this weakens the compatibility of mmWave band for carrying out communication operations [44].

3.1.4 Interference

The employment of the steerable links that are vulnerable to blockages by obstacles due to the propagation characteristics will considerably expose mmWave system to a type of disruption with on-off behavior. The competition among the new approaches and criterions to occupy open access frequencies, cohabitation of licensed and unlicensed bands in 5G system is creating an unpredictable interference in mmWave band in both spectral and spatial domains [45].

3.1.5 Impulsive Noise

Based on the source, noise may exist in various electrical frameworks in different manifestations. It is often dominated by the Gaussian distribution model which is ruled by the central limit theorem. Though, the Gaussian noise has a bad influence on communication process, its effect is not exceeding a hiss on transmitting channels, which fulfills a maintained level of intelligibility in communication system. Nonetheless, numerous physical channels have been exposed to some sorts of clicks that would harm the intelligibility and degrade the communication system. This originates from a non-Gaussian behavior, in particular, IN [37, 46, 47].

IN is composed of sudden sharp bursts as a sequence form of “on/off” random pulses in the time domain. It is generated naturally in the atmosphere as electrical discharges caused by thunderstorms and produced by man-made noise sources as a sort of high-voltage powerline discharge, switching-engine noise in electrical motors, and ignition noise in vehicles and aircraft. Moreover, IN is the overriding noise in wireline telephone channels and it can be considered an irritation factor in voice

transmission implementations. Likewise, it is arisen through a mobility system by radio frequency interference when it comes to receiving antennas associated with highly intense transmitter medium within metropolitans [36, 37, 46].

3.1.5.1 Impulsive Noise Characteristics

Contravening the ordinary pulse that has momentary steady spectrum over the frequency band and remains for minuscule short time, IN is typically non-stationary short duration bursts that arise randomly in time and space, and then diffuse within the channel to the receiver. The occupation of slight impulses per second to measure the power spectrum for IN reveals its non-stationary nature through the zero valued power when noise is missing and the power value of impulse otherwise [36, 47].

Revealing the characteristics of IN arises from three frameworks: IN modelling, detection and reduction. Intrinsically, modelling of IN enriches the existing realization of its sources and submits a pragmatic and quantitative illustration of such type of perturbation. The recognition of IN modeling comprises the fundamental coefficients and the associated probability density functions [48, 49].

The IN burst often takes the form of a declining vacillating non-zero duration impulse exemplified by more than one sample long. Figure 3.1 illustrates some examples of the varying channel properties in a varying period versus the impulsive amplitudes, where $n_i(m)$ is the amplitude modulated binary state sequence for m impulsive sequence. Figure 3.2 displays the main parameters of IN burst.

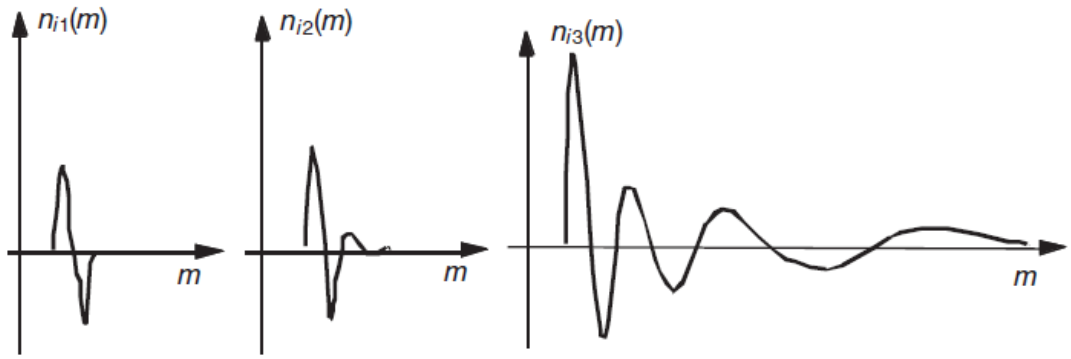

Figure 3.1: Illustration of IN bursts

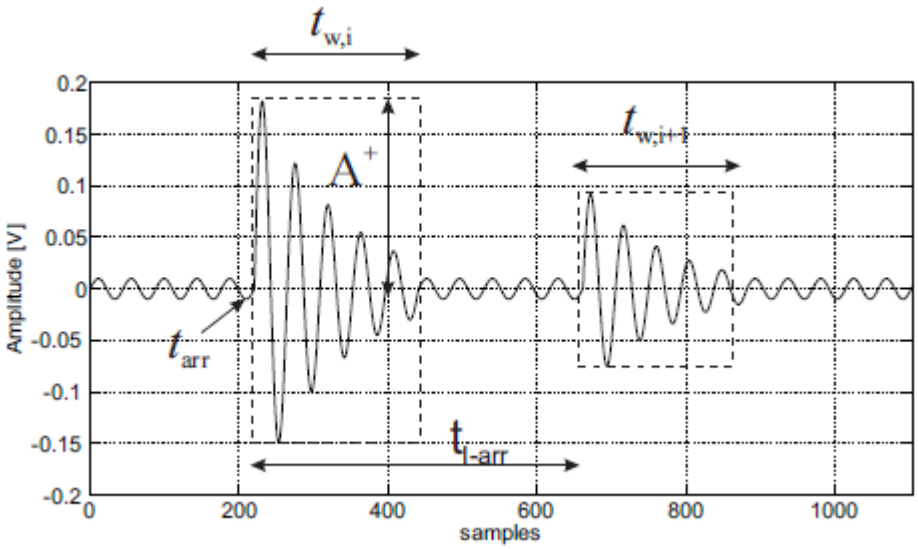

Figure 3.2: IN main parameters

The IN parameters shown in Figure 3.2 are peak amplitude (A^+), width (t_w), arrival time (t_{arr}) , and inter-arrival time (t_{l-arr}) which is the time between successive bursts [36, 48].

3.1.5.2 Impulsive Noise Models

Over a large monitoring time, IN is modeled by consecutive short impulsive events with additive background noise and recognized by its instant amplitude probability density function. Further, it is resulted from an overlaying of many autonomous

sources combined with random amount of impulsive emissions and their overall sites are randomly disseminated in space. It is given by:

$$x(t) = \sum_k u_k(\theta_k, t) \tag{3.1}$$

where $u_k(\theta_k, t)$ is the k^{th} interferer and θ is the set of random variables characterizing the interference. Various existing patterns have been evolved to depict IN, namely, as follows [49]:

3.1.5.2.1 Middleton Model

To emulate the non-linearity of electro-magnetic interference while bearing in mind the Gaussian component as a representation for thermal noise at receiver, Middleton has developed three statistical models. Middleton class A, B and C noise models present a vast, canonical visualization of many non-Gaussian operations in different environments [46, 50].

When the transients in a typical receiver are ignored, class A model is implemented for narrowband chaos. However, class B handles the transients of receiver and broad noise in more complicated form than class A, while class C is the mixture between the aforementioned models.

The power density function (pdf) of class A noise is given by:

$$f_{P+G}(x) = e^{-A} \sum_{m=0}^{\infty} \frac{A^m}{m!\sqrt{2\pi\sigma_m^2}} e^{\frac{-x^2}{2\sigma_m^2}} \tag{3.2}$$

where A is the impulse index, the average number of simultaneously active impulsive origins, σ_m^2 is calculated as $\frac{\frac{m}{A}+\Gamma}{1+\Gamma}$ where $\Gamma \in [10^{-6}, 1]$ is the ratio between the level of background noise and IN [49].

3.1.5.2.2 Symmetric Alpha Stable (SαS) Model

This model exhibits a fine behavior in supporting the generalized limit theorem and is utilized to model the heavy-tailed IN distributions. It supports modeling IN sources by exploiting different rational and tentative approaches. It is considered a substitutional model for estimation Middleton class B model. However, it does not have closed-form expressions due to their complex derivations, excluding some values disclosed in the following characteristic function:

$$\phi_x(w) = e^{-\gamma|w|^\alpha} \tag{3.3}$$

where γ gauges the expansion of distribution around its center, and α is the stability factor that measures the intensity of distribution tail where for $\alpha = 1$, pdf is Cauchy distribution, for $\alpha = 2$, pdf is Gaussian distribution and for $\alpha = \frac{1}{2}$, pdf is Levy distribution [46, 49].

3.1.5.2.3 Markov Model

It has been harnessed in many environments when IN shows an intermittent attitude. In spite that this model has diverse schemes and patterns, however, they are all based on a set of steady transition state probabilities tied with the absence and existence of IN [36, 49].

3.1.5.2.4 Gaussian Mixture Model

The Gaussian mixture model is founded to roughly guesstimate any given density. By referring to density approximation theorem, the non-Gaussian noise distribution can be demonstrated through a quantified summation of Gaussian distributions of proper mean vectors and covariance matrices. The general form of mixture model with *K* components is given by:

$$f_{GM}(x) = \sum_{i=1}^{K} c_i \, f_G(x, \mu_i, \sigma_i^2) \tag{3.4}$$

where c_i is the weight coefficient vector and $f_G(x, \mu_i, \sigma_i^2)$ is the Gaussian pdf with mean μ_i and variance σ_i^2 vectors [36, 51].

Nonetheless, the form of Gaussian mixture model which is most frequently used is defined as the ε-mixture model, where the noise density function is expressed as

$$f(x) = (1 - \varepsilon) f_b(x) + \varepsilon f_o(x) \tag{3.5}$$

where $\varepsilon \in [0,1]$ is the mixture parameter which adjusts the occurrence of IN, $f_b(x)$ represents the Gaussian background noise with variance σ_b^2, $f_o(x)$ designates the contaminating IN with variance σ_o^2. The value of the ratio $p = \frac{\sigma_o^2}{\sigma_b^2}$ lies between 1 and 10,000.

Due to its empirical simplicity and elasticity, the mixture model has been utilized in approximating many diverse symmetrical distributions, moreover, it is exploited to simulate the non-Gaussian gauging channels in narrowband interference mitigation. The model for IN as a mixture of five Gaussian pdfs is depicted in Figure 3.3 [46, 51].

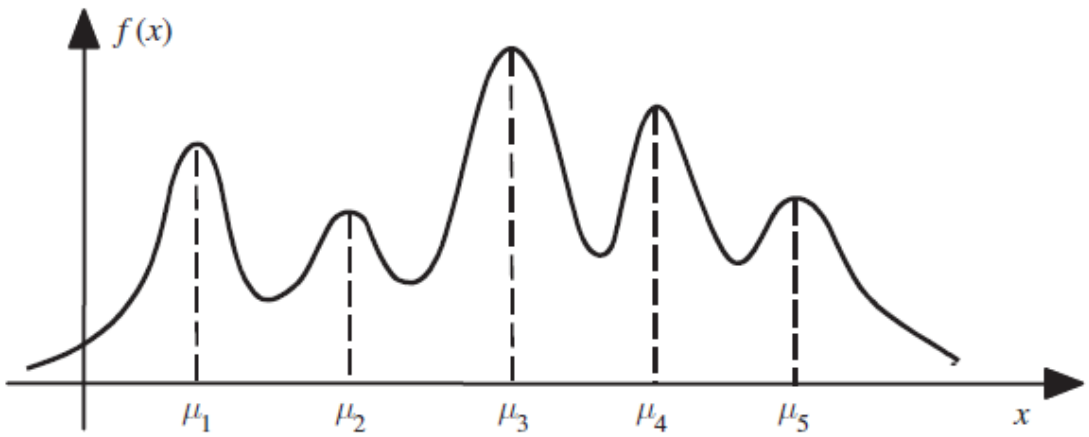

Figure 3.3: A Gaussian mixture model pdf [36]

3.1.5.3 Impulsive Noise Presence in High Frequencies

There is no direct proof for IN existence at mmWave frequencies band and none of any previous study tackles the problem either. However, many researches gave some evidence for the presence of IN at the band of high frequencies in its several shapes: man-made noise, electromagnetic interference, non-Gaussian clutter, and nonstationary chaos.

3.1.5.3.1 Impulsive Radio Interference

Radio noise is restricting the performance of communication systems through its variant sources: atmospheric noise due to lightening, atmospheric gases emissions, obstructions within antenna beams, celestial radio radiation and man-made noise. The impulsive components exist in 1 Hz up to 1 GHz frequency band. However above 1 GHz, the external noise figure (F_a) will be low and only a few pulses with the higher magnitude will remain. Nevertheless, these values were measured in the 1970s and may change with time, depending on the activities which may generate man-made noise.

Figure 3.4 illustrates the performance of various types of radio noise interpreted by F_a in the band 100 MHz up to 100 GHz. A denotes the business area man made noise, B exemplifies the galactic noise, C represents the galactic noise with infinite narrow beam, D denotes the quiet sun noise, E is the sky noise with upper (90^o elevation angle) and lower (0^o elevation angle) curves and F represents the cosmic noise. [52].

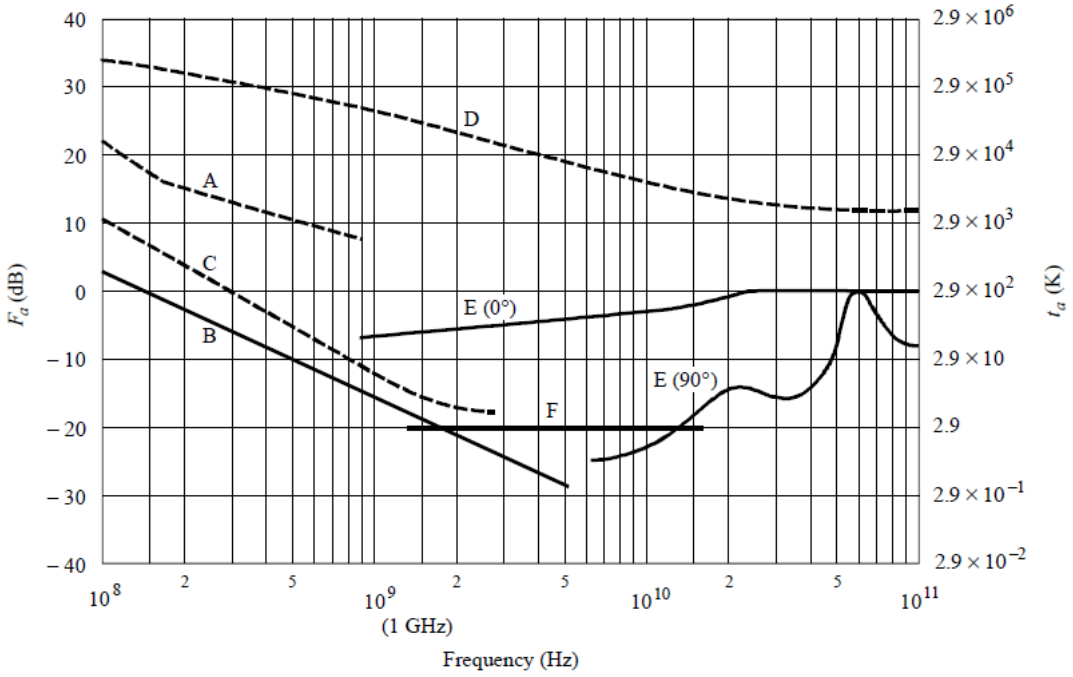

Figure 3.4: F_a versus frequency for radio noise's individual sources [52]

3.1.5.3.2 Impulsive Noise within Electrical Substations

At 6 GHz, IN is diffusing within high voltage electricity substations and has the capability to break down their functionality. It further frustrates implementing the practical wireless technologies used in the electricity supply industry [53].

3.1.5.3.3 Impulsiveness in Global Positioning System

Global Positioning System (GPS) receiver is exposed to noise and multipath. In spite of the fixed pulse amplitude and steady intervals of transmission, multipath fetches the randomness to GPS receiver. Further within the receiver, transmitting the repeated short pulses in ultra-wideband systems conduce the undesired impulsiveness. This IN may contaminate GPS signals and brings out crucial tracking errors. It overlaps with GPS band within an approximate frequency range of 100 MHz –10 GHz [54].

3.1.5.3.4 Impulsiveness in Optical Fiber Transmission System

In a 12 GHz 64-Quadrature Amplitude Modulation (QAM) signal in a hybrid Amplitude Modulation-Vestigial Side-Band AM-VSB/64QAM optical fiber transmission system, the impulsive components that are caused by the nonlinearity of the laser diode would distribute over a wide spectrum. They interfere with digital signals in a QAM channel and degrade the hybrid system [55]. On the other hand, at 20 GHz, a distortion with an impulsive behavior affects both AM and 16QAM signal transmission systems and degrade Bit Error Rate (BER) of 16QAM signal in AM/16QAM hybrid optical transmission system [56].

3.1.5.3.5 Additive White Generalized Gaussian Noise

The performance of mmWave Weibull fading channels in wireless systems is unsettled by the impact of Additive White Generalized Gaussian Noise (AWGGN). AWGGN is vastly used to model additive noise in many implementations in engineering and science. It comprises several sorts of noise such as impulsive, uniform, Gaussian, and Laplacian noises that may promote the fluctuation of the peakedness parameter of the signal distribution and cause severe degradation in the system [57].

3.1.5.3.6 Impulsive Clutter in Radar System

The Non-Gaussian clutter is often observed to be spiky in a radar system. In most cases, the weak detection capability for the Gaussian receiver frustrates its sensing about the non-Gaussian clicks, especially for weak target returns [58]. The amplitude statistic of high-resolution radar's clutter shows large deviations from the Rayleigh distribution which makes the classical Gaussian model inappropriate to model such interference [59]. Nevertheless, to model the impulsive clutter in a radar system, an alpha-stable with complex random process is used through developing a joint target

angle and Doppler, maximum likelihood-based estimation techniques [60]. Therefore, the ambient noise in many physical radar environments has been recognized as non-Gaussian. It is found further that the performance of the airborne military radars and obstacle detection radars (35 GHz) hanged with helicopters, besides the automotive radars (77 GHz) and traffic monitoring radars (24 GHz) are all affected negatively by the presence of IN [61].

mmWave radar-based sensors are exploited in many automotive applications including obstacle detection and collision warning, true-speed, and road-surface recognition. However, the system doesn't perform properly due to the shortage of precise knowledge of the clutter attitude, particularly, in the highway environment. When asphalt road surfaces are possibly covered with ice or water, they are interacting with electromagnetic waves at 94 GHz [62].

3.1.5.3.7 Impulsive Randomness in Beamforming

A robust new beamforming technique has been improved to mitigate the impulsive random errors with a heavy-tailed distribution which contaminate the complex-valued observations for beamformer at high frequencies [63].

3.1.5.4 Impulsive Noise Impact on Directional Arrivals (Angle of Arrival)

It is noticeable that the outputs of the array elements become steadily more incompatible as the angular range of noise sources grows. Primarily, if the array elements power is a function of Directional of Arrivals (DOA), and meanwhile the power is constant or slowly altering under the effect of noise. Therefore, it is obvious that DOA is exposed to noise impact [32].

Due to the exponential increment of cellular data traffic, the electromagnetic environment has become more complex gradually. The interference sources in such an environment contain natural and human-made. It can also be exhibited as a low-frequency atmospheric noise and underwater acoustic signal. While often in wireless systems, the channel noise usually appears in a non-Gaussian form that always reveals the impulsive characteristics, such as random pulses and sharp spikes. Under such circumstances, DOA estimation techniques severely deteriorate in the presence of impulsive noise. As a consequence of their heavy tails, IN amplitude causes massive shifts out of the average in DOA gauging more than the Gaussian noise [64, 65].

Chapter 4

NONLINEAR PREPROCESSORS IN IMPULSIVE NOISE MITIGATION IN MMWAVE SYSTEM

The nonstationary attitude of IN creates the devastating unpredictable effect on communication channels. Further, it is even more complicated than the behavior of Gaussian noise when it is subjected to investigation. It was therefore necessary to find efficient strategies and approaches to minimize its destructive impact. Through different studies over many cellular systems, clipping, blanking and hybrid filters are the simplest and the most effective techniques to suppress the adverse impact of IN [66, 67]. This chapter inspects the implementation of the clipping, blanking and hybrid preprocessors over mmWave massive MIMO system contaminated with IN. The presented algorithms for the abovementioned preprocessors are applied to conquer IN impact on the proposed system.

In spite of its solidity and efficiency in the wireless network, mmWave system is subject to many sorts of attenuation and noise. The effect of phase noise on mmWave cellular system is displayed in a 120 GHz mmWave system with two lasers and two Mach–Zehnder modulation utilizing frequency 8-magnitudes of RF local oscillator's signal frequency. Fiber optical Bragg Grating techniques are used to prevent phase noise and slight BER [68]. Whereas in [69] a phase noise analysis and measurements in a W-band Frequency-Modulated Continuous-Wave (FMCW) radar prototype is presented. It reveals the elimination of phase noise to a high extent of about 40 dB at

1 MHz based on performing a high transmit/receive isolation and a feed-forward circuit structure. On the other hand, the performance of an optically-connected mmWave radar system in [70] is practically gauged by comparing two sorts of signal generators for computing the impact of signal-source phase noise. A 96 GHz FMCW signal is generated by multiplying a 4 GHz signal resulting in a 10 dB reduction of phase noise. Detecting the presence of thermal noise in mmWave system is estimated in [71] through the interference-to-noise ratio by the latest measurement-based statistical channel models considering blockage, LOS and NLOS schemes as well as local scattering. Interference is recognized through the MAC protocol which may exemplify the proper solution to better uplift mmWave potential. While in [72], a W-band waveguide radiometer at the range of 75 GHz to 105 GHz was built to quantify the radiated noise power throughout the calculation of the excess noise ratio within a diode noise source. It shows that the thermal noise can be distinguished in the aforementioned frequency band, however, the radiometer needs more enhancement above 105 GHz. During channelization, some defects cause an inter-band interference in an indoor mmWave system in [73] that may waste energy and cost. By employing the analogue to digital conversion, the inter-band interference is imposingly minimized by the adaptive linear Minimum Mean Squared Error techniques for joint capture across contiguous subbands. Meanwhile, a random antenna selection scheme is proposed in [74] to minimize the inter-user interference in multi-user mmWave beamforming systems. Using the Gaussian approximation, the results reveal that the inter-user interference is mitigated and beamforming with random antenna selection can get the benefit of a large array. In mmWave Schottky detectors [75], the flicker noise is detected. By the technique of differentiating between direct current and RF current distribution at the quasi vertical structure for

diode, the results depict a good flicker noise prediction for Schottky detectors. Besides, there are other several studies devoted to many forms of noise and attenuation in a mmWave system [76-79].

Based on the above-mentioned methods and techniques, all of the previous studies do not address the presence of IN in mmWave system. Furthermore, the exploitation of clipping, blanking and hybrid preprocessors for IN mitigation was limited to Power Line Communications (PLC) and MIMO systems and never been investigated on mmWave communications system. Consequently, because of its harmful effect on the wireless system and its constituents, including mmWave technology, there is a need to examine the effect of IN on mmWave communications systems. Fortunately, by relying on the hypothesis previously mentioned in Chapter 3, IN was detected at the lower band of mmWave frequencies. Moreover, IN suppression was verified primarily by implementing blanking and clipping filters in a mmWave system through [80].

4.1 System Model

To examine the performance of the non-linear units in a mmWave system impaired by the impulsive environment, the mmWave transceiver model and the nonlinear preprocessors model are used here. The transceiver model depicts the downlink BS receiver for mmWave system. While the preprocessors model is the most efficient model used for tackling IN. It is placed at the front end of the transceiver model and implemented for clipping, blanking and hybrid functions.

4.1.1 mmWave Massive MIMO Model

A common mmWave system receiver has a configuration where the array signal processing is partitioned into RF combiners followed by baseband combiners. The

RF precoder and combiner monitors the phases of the signals that pass through pure analog phase shifters into and out of the antenna elements to produce multiple beams in the direction of the dominant paths in the mmWave field. Every antenna element at the BS involves one RF chain, in which an RF chain includes a low-noise amplifier, downconverter and a digital to analog converter. The baseband precoder, meanwhile, provides an additional level of flexibility over the constant-gain/phase-only operations at the RF precoder. The precoders are $\mathbf{F}_{RF}$ and $\mathbf{F}_{BB}$ which are built by BS to approximate the dominant singular vectors of the channel. Whereas the combiners $\mathbf{W}_{RF}$ and $\mathbf{W}_{BB}$ are built in MS or the receiver.

The simplified block diagram of the proposed receiver model of downlink mmWave communications system with large antenna arrays at both BS and MS is shown in Figure 4.1.

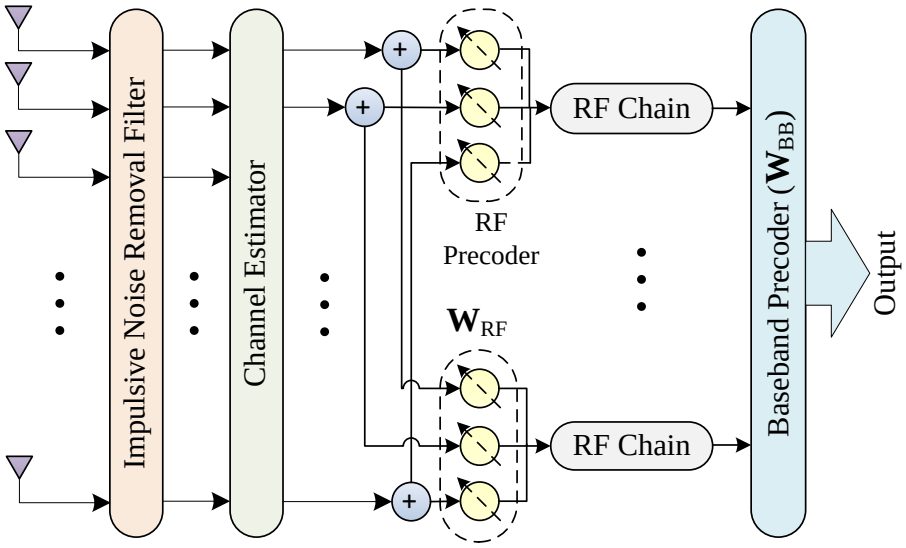

Figure 4.1: Simplified BS receiver block diagram of mmWave system

In this model, a BS with N_{BS} antennas and N_{RF} RF chains communicates with an MS having N_{MS} antennas and N_{RF} RF chains. BS communicates with MSs via N_S data streams as described in [81]. An $N_{RF} \times N_S$ baseband precoder, $\mathbf{F}_{BB}$ is assumed to be applied at BS followed by an $N_{BS} \times N_{RF}$ RF precoder, $\mathbf{F}_{RF}$. The combined BS precoding matrix, $\mathbf{F}_T = \mathbf{F}_{RF}\mathbf{F}_{BB}$ with dimensions $N_{BS} \times N_S$ is formed to yield a discrete-time transmitted signal:

$$\mathbf{x} = \mathbf{F}_T\mathbf{s} \tag{4.1}$$

where **s** is the transmitted symbol vector of dimension $N_S \times 1$. The constant modulus entries of $\mathbf{F}_{RF}$ implemented using analog phase shifters satisfies $|[\mathbf{F}_{RF}]_{m.n}|^2 = N_{BS}^{-1}$, where $|[\mathbf{F}_{RF}]_{m.n}|$ denotes the magnitude of the $(m,n)^{th}$ element of $\mathbf{F}_{RF}$. The received signal at the output of the narrowband block-fading channel that would be observed by MS is then:

$$\mathbf{r} = \mathbf{H}\mathbf{F}_\mathbf{T}\mathbf{s} + \mathbf{n} \tag{4.2}$$

where **H** is mmWave channel matrix of $N_{MS} \times N_{BS}$ elements between MS and BS as defined in [81–83], and **n** is the overall noise corrupting the received signal. The discrete-time narrowband channel **H** with L paths can be written as:

$$\mathbf{H} = \sqrt{\frac{N_{BS}\, N_{MS}}{\rho}} \sum_{l=1}^{L} \alpha_l \mathbf{a}_{MS}(\theta_l)\mathbf{a}_{BS}^{H}(\phi_l) \tag{4.3}$$

where ρ denotes the average path-loss between BS and MS and α_l is the complex gain of the l^{th} path. The variables θ_l and $\phi_l \in [0,2\pi]$ are the l^{th} path's angels of arrival and departure respectively. The vectors $\mathbf{a}_{MS}$ and $\mathbf{a}_{BS}$ represent the normalized received and transmit response vectors at an angle of θ_l and ϕ_l respectively.

In this system, we employed ULA antenna architecture. This architecture is a collection of sensor elements such as dipole antennas, spaced along a straight line by

a distance equal or less than the half of the wavelength. ULA antenna structure is used to improve SNR and gain in a particular direction. Assigning one RF chain to each antenna consumes a huge amount of power, thus usually hybrid beamforming is used with a limited number of RF chains to reduce the cost and power consumption.

The received signal **r** can then be obtained by processing the signal at MS by $\mathbf{W}_T = \mathbf{W}_{RF}\mathbf{W}_{BB}$ as:

$$\mathbf{y} = \mathbf{W}_T^H \mathbf{H}\mathbf{F}_T\mathbf{s} + \mathbf{W}_T^H \mathbf{n} \tag{4.4}$$

where $\mathbf{W}_T$ is composed of RF and based-band combiners $\mathbf{W}_{RF}$ and $\mathbf{W}_{BB}$ respectively. **n** is modeled by Gaussian mixture model which is an approximation of Middleton class-A noise model [84] that can be written as:

$$\mathbf{n} = \mathbf{w} + \mathbf{z} \tag{4.5}$$

where **w** and **z** represent the complex Additive White Gaussian Noise (AWGN) and IN.

4.1.2 Impulsive Noise Model

IN shows an abrupt random time attitude besides the fluctuating duration from a few microseconds to milliseconds. During the realistic events, Power Spectral Density (PSD) of IN surpasses PSD of background Gaussian noise with at least 10-15 dB and may sometimes reach 50 dB [85]. As provided in Section 3.1.5.3, mmWave low-frequency band experiences the hazardous presence of IN. However, Figure 4.2 illustrates the time-domain representation of a number of impulses together with the background Gaussian noise with an overall duration of 0.8 ms.

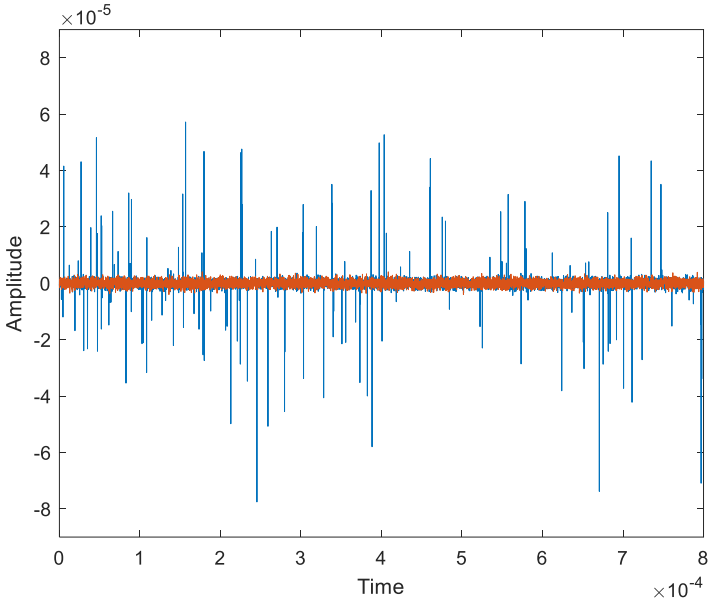

Figure 4.2: IN mixed with Gaussian noise in time domain

IN occurs with a probability of ϵ. Assuming that the Gaussian terms are denoted as $N(0, \sigma_w^2)$ and $N(0, \sigma_z^2)$, the mixture distribution of the total noise has the following form:

$$f = (1 - \epsilon)N(0, \sigma_w^2) + \epsilon N(0, \sigma_z^2) \tag{4.6}$$

where $N(.)$ is the Gaussian probability density function, σ_w^2 and σ_z^2 denote the variances of AWGN and IN, which are related to the input SNR and Signal to Impulsive Noise Ratio (SINR), respectively.

4.1.3 Non-Linear Preprocessors

In the high IN ambiences, nonlinear preprocessors are operating as memoryless time-domain devices at the front end of the receiver. Since they are uncomplicated appliances, they have been frequently used in the feasible applications. It is postulated that the amplitudes of IN are often discriminately higher than the signal amplitudes, thus a threshold should be designated. When the signal amplitudes exceed the nominated threshold, they are supposed to be contaminated and hence

adjusted based on the functioning preprocessor. Specifically, the affected values are assigned by threshold values in clipping, while in blanking they are zeroed [86,87].
In PLC, clipping and blanking are considered a straightforward way to reduce IN. A precoding matrix at the transmitter in [88] is improving SNR and the performance of blanking; besides it lessens the false alarms in detecting IN. However, in [89-91] the probability of missed clipping/blanking is minimized to enhance the performance of the system. Otherwise, the proposed schemes can achieve better SNR performance than conventional techniques.

Every so often in PLC, blanking preprocessor performance is disrupted by the harmful internal interference due to its nonlinearity. As a result, an enhanced version is proposed to combat such effects, gaining a better 1-4 dB SNR for variant impulsive environments [92]. For an OFDM-based system, the core of the proposed adaptive technique is to find the appropriate method for reducing IN based on using a level detector with a set of thresholds. The technique offers improved BER performance compared to conventional techniques [93]. Whereas an OFDM receiver in [94] employs an adaptive blanking threshold calculation with a capability to handle sorts of impulsive interference. The proposed technique can be applicable for a wide range of OFDM systems based on the iterative structure of blanking nonlinearity besides the frequency selective blanking nonlinearity.

The structure of periodic pulse train function and Fourier series controls the measurement of semi optimal thresholds for blanking and clipping preprocessors in many simple techniques. The ideal design of optimal thresholds is identical with the error performance for the nonlinearity preprocessors in OFDM receiver [95]. In order to set a clipping level, the average of the received signal samples is measured.

However, [96] outperformed the other schemes regarding SNR and symbol error rate values.

Without harnessing IN statistics, an approach was conducted in [97] to mitigate the error floor through deriving and formulating clipping threshold as a pairwise error probability optimization problem. It imitated the Maximum Likelihood decoder performance at high SNR under Bernoulli Gaussian noise model with a wide range of parameters. On the other hand, the Cauchy distribution was utilized in [98] for attaining the optimum clipping threshold. By applying density evolution tool, clipping de-mapper slope is adjusted; otherwise, the clipping de-mapper gained a satisfactory performance. Hybrid preprocessor proved its efficiency to suppress IN through [99-102]. Besides, literature in [102-108] tackled the implementation of clipping, blanking, and hybrid filters for a contaminated impulsive environment in different systems.

4.1.3.1 Conventional Nonlinear Preprocessors

Commonly, they comprise the following:

- **Clipping Preprocessor**

Any signal amplitude overrides the value of clipping threshold (T_c) is assumed to be corrupted by IN, and forthwith its amplitude is altered to T_c. Even though both amplitude and phase are detected by clipping filter, however, phase remains constant and the amplitude will be modified as:

$$y_k = \begin{cases} r_k, & |r_k| \leq T_c \\ T_c e^{jarg(r_k)}, & |r_k| > T_c \end{cases}, \quad k = 0, 1, \dots, N-1 \tag{4.7}$$

where r_k and y_k are the input and output of the nonlinear filter, respectively.

- **Blanking Preprocessor**

Similar to clipping filter, the uncontaminated signal remains as it is as long as it is not overriding the threshold value. While in blanking filter, any amplitude of signal sample surpasses the blanking threshold value (T_b) will lead into a zero-valued signal and the phase is kept unchanged as:

$$y_k = \begin{cases} r_k, & |r_k| \leq T_b \\ 0, & |r_k| > T_b \end{cases}, \ k = 0, 1, \dots, N-1 \tag{4.8}$$

- **Hybrid Preprocessor**

Hybrid preprocessor is the conjunction between clipping and blanking preprocessors, where two thresholds are defined; clipping threshold T_1 and blanking threshold T_2 ($T_1 \leq T_2$). When the amplitude of a signal sample is overriding the blanking threshold T_2, the sample is altered into zero. Meanwhile, the signal sample is clipped and designated by T_1 value if it is below the blanking threshold T_2 and still above the clipping threshold T_1. Otherwise, the rest of signal samples with amplitudes below the clipping threshold are left without adjustment.

$$y_k = \begin{cases} r_k, & |r_k| \leq T_1 \\ T_1 e^{jarg(r_k)}, & T_1 < |r_k| \leq T_2, \\ 0, & |r_k| > T_2 \end{cases} \ k = 0, 1, \dots, N-1 \tag{4.9}$$

Based on the abovementioned and the researches in [86-108], it is noticeable that the nonlinear filters are adjusting amplitudes and retaining the values of the phases of the processed signals. This due to the fact that nonlinear filters are diode-based circuits, their output signals are essentially direct current or modulated direct current associated with amplitude modulation which do not contain phase information. The voltages on the terminals of the diode limiter circuit are altered to provide a uniform rectangular pulse for interrupting and reducing the noise bursts [109-112].

4.2 Impulsive Noise Removal Filters Model in mmWave System

In front of the receiver, the received signal **r**, represented by (4.2) is passed through IN removal filter with blanking or clipping functions as shown in Figure 4.3.

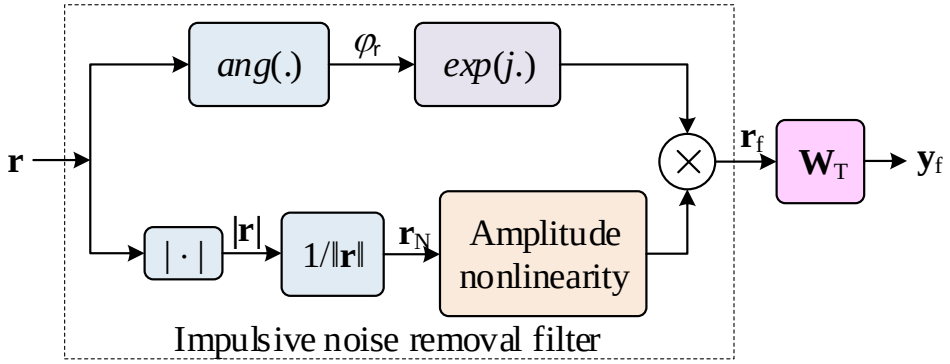

Figure. 4.3: Block Diagram of the Nonlinear Preprocessor at the Receiver

At the filter, the absolute values of the elements of the received signal vector **r** are normalized by dividing them with their norms as:

$$r_{\mathrm{N}}(i) = |r(i)|/\|\mathbf{r}\| \tag{4.10}$$

where $|r(i)|$ represents the absolute value of the i^{th} component of the vector **r,** and $\|\mathbf{r}\|$ denotes the norm of vector **r**. The noise removal filter is used to detect the amplitude and the phase of the received signal to yield the filtered received signal by modifying the amplitude while keeping the phase unchanged.

In order to optimize the system performance, the filter thresholds need to be selected carefully. With the choice of a proper threshold and multiplying the received signal with the combiner matrix $\mathbf{W}_{\mathrm{T}}^{H}$, the filtered received signal at the combiner output becomes [81]:

$$\mathbf{y}_{\mathrm{f}} = \mathbf{W}_{\mathrm{T}}^{H}\mathbf{r}_{\mathrm{f}} \tag{4.11}$$

where $\mathbf{r}_\mathrm{f}$ is the filtered received signal, and $\mathbf{y}_\mathrm{f}$ is the output processed received signal at MS.

4.2.1 Clipping Filter

If the amplitude of the i^{th} element of normalized received signal vector $r_\mathrm{N}(i)$ is greater than T_c, the output of the clipping filter is limited to $T_\mathrm{c}\|\mathbf{r}\|$, otherwise, it is left unattended as:

$$r_\mathrm{c}(i)=\begin{cases} T_\mathrm{c}\|\mathbf{r}\|, & r_\mathrm{N}(i) > T_\mathrm{c} \\ r(i), & r_\mathrm{N}(i) \le T_\mathrm{c} \end{cases} \tag{4.12}$$

Then, the filtered received signal $\mathbf{r}_\mathrm{f}$ is constructed as:

$$\mathbf{r}_\mathrm{f} = \mathbf{r}_\mathrm{c} e^{-j\varphi_r} \tag{4.13}$$

where T_c is the clipping threshold and $\boldsymbol{\varphi}_\mathrm{r}$ is the phase angle of the received signal vector $\mathbf{r}$.

4.2.2 Blanking Filter

Whenever the amplitude of the i^{th} element of the normalized received signal vector $r_\mathrm{N}(i)$ is greater than T_b, the output of the blanking filter is set to zero, otherwise, it is left unattended as:

$$r_\mathrm{b}(i)=\begin{cases} 0, & r_\mathrm{N}(i) > T_\mathrm{b} \\ r(i), & r_\mathrm{N}(i) \le T_\mathrm{b} \end{cases} \tag{4.14}$$

Then, the filtered received signal $\mathbf{r}_\mathrm{f}$ is constructed as:

$$\mathbf{r}_\mathrm{f} = \mathbf{r}_\mathrm{b} e^{-j\varphi_r} \tag{4.15}$$

where T_b is the blanking threshold.

4.2.3 Hybrid Filter

If the amplitude of the i^{th} element of normalized received signal vector $r_\mathrm{N}(i)$ is greater than T_2, the output of the hybrid filter is set to zero. While the output of the filter is limited to $T_1\|\mathbf{r}\|$ whenever the amplitude of the i^{th} element of $r_\mathrm{N}(i)$ is greater than T_1 and yet below T_2. Otherwise, it is left unmodified as:

$$r_{\mathrm{h}}(i)=\begin{cases} r(i), & r_{\mathrm{N}}(i)\le T_1 \\ T_1\|\mathbf{r}\|, & T_1 < r_{\mathrm{N}}(i)\le T_2,\ k=0,1,\ldots,N-1 \\ 0, & r_{\mathrm{N}}(i) > T_2 \end{cases} \tag{4.16}$$

Then, the filtered received signal $\mathbf{r}_{\mathrm{f}}$ is constructed as:

$$\mathbf{r}_{\mathrm{f}} = \mathbf{r}_{\mathrm{h}} e^{-j\varphi_r} \tag{4.17}$$

where T_1 is clipping threshold and T_2 is blanking threshold; $T_2 = KT_1$, where K is a proportionality constant ($K > 1$) [86, 87, 102].

Chapter 5

SIMULATION RESULTS

To assess the performance of the system, the downlink mmWave communications system shown in Figure 4.1 is simulated in MATLAB with N_{BS} = 64 antennas and 16 RF chains at BS communicating with N_{MS} = 32 antennas and 8 RF chains at MS. Uniform linear array model is employed for the antenna arrays where the antennas are separated by half wavelength distances. We consider the channel model defined in (5.3) with L=3 paths whose amplitudes are assumed to be Rayleigh distributed with an average power gain of 1 and path-loss exponent of 3. Although the system is designed to operate between 3-300 GHz mmWave frequency band, it is tested at 28 GHz carrier frequency with a bandwidth of 100 MHz. The hybrid precoding matrices are constructed as defined in [81] using the structure of multi-resolution codebook with a resolution parameter of 192 having 2 beamforming vectors in each subset. The distance between the transmitter and receiver is set to 50 meters throughout the simulations. The simulation parameters are set for the signaling as 16-QAM (M=16) unless stated otherwise and for IN channels SINR is kept constant as -10 dB. Each simulation scenario is repeated 1000 times to achieve an average performance in every setup.

5.1 Impulsive Noise Impact on mmWave System

Fig 5.1 shows the performance of mmWave communication system under Gaussian noise and IN. Relying on the two scenarios devoted to IN at ϵ = 0.02, ϵ = 0.04, it is

obvious that when the ϵ increases, this will elevate the cruel impulsiveness impact on the system gradually.

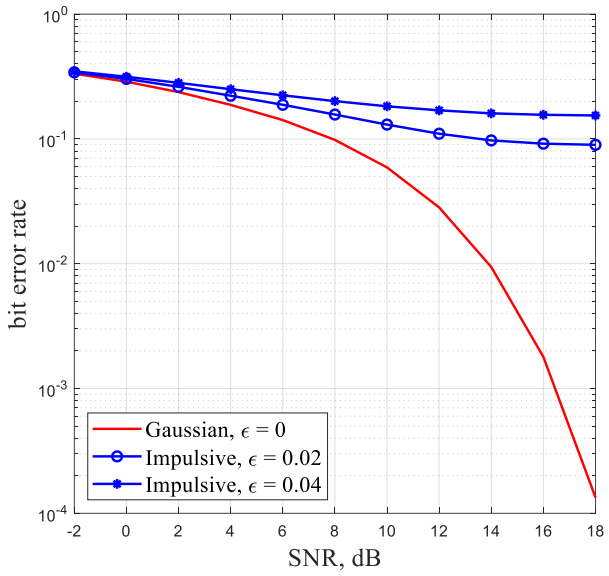

Figure 5.1: BER of mmWave system versus SNR under Gaussian (ϵ = 0) and IN (ϵ = 0.02, ϵ = 0.04)

5.2 Performance Analysis for Fixed Threshold

It is important to find the peak threshold value for clipping and blanking filters in order to estimate their capabilities in IN reduction and minimizing BER. Selecting the optimum threshold value ensures suppressing IN while not removing useful signal content along with IN.

Figs. 5.2 and 5.3 show how BER changes with different blanking thresholds under IN for clipping and blanking at ϵ = 0.02 for different SNR values. It is shown that for every SNR, there is an ideal threshold that minimizes BER.

At ϵ = 0.02, it is noticed from Figure 5.2 that for the blanking filter there is a considerable minimum BER enhancement from 7×10^{-3} to 9.9×10^{-4} when T_{b}

equals 0.3 when SNR=20 dB. While in Figure 5.3, clipping filter doesn't override blanking, however, it performs a BER minimization from 2.2×10^{-2} to 6.3×10^{-3} at T_c = 0.18 and 20 dB SNR.

Otherwise, the performance of the preprocessors will change when increasing the probability of impulsive pulses to 0.04. Blanking gains a minimum BER of 6×10^{-3} when T_b equals 0.27 in Figure 5.4 and outperforms the clipping filter which attains 2×10^{-2} at T_c = 0.16 and SNR=20 dB illustrated by Figure 5.5.

Figs. 5.4 and 5.5 similarly present BER against blanking and clipping thresholds at ϵ = 0.04. As clearly observed from the results presented in Figure 5.2 to 5.5, the best performance is achieved with the filters at a certain threshold value.

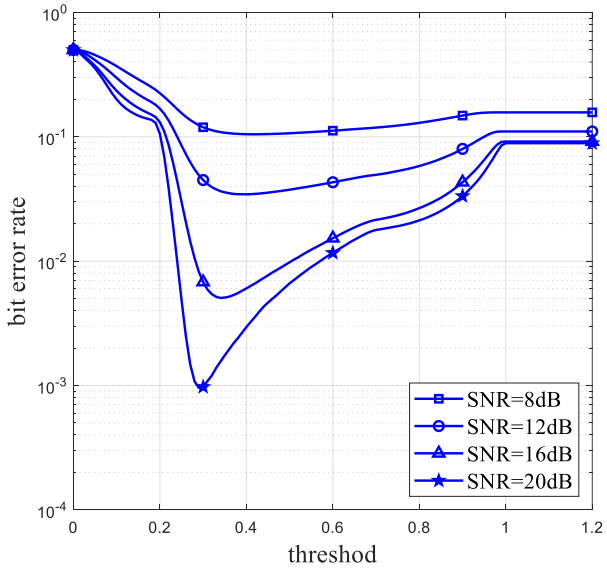

Figure 5.2: BER against blanking threshold under IN (ϵ = 0.02)

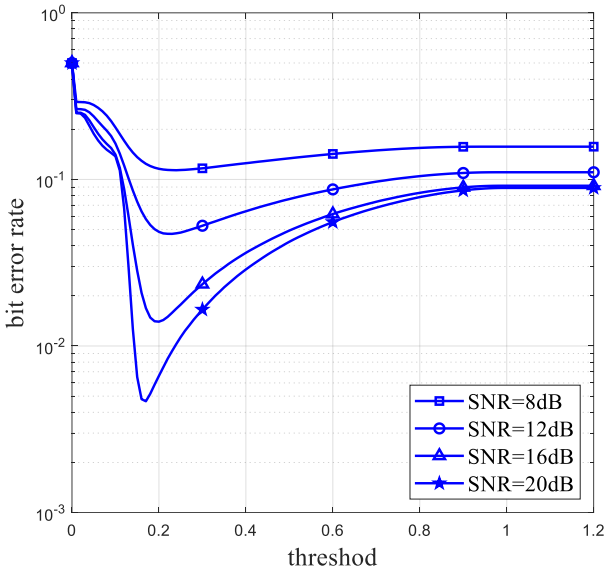

Figure 5.3: BER against clipping threshold under IN (ϵ = 0.02)

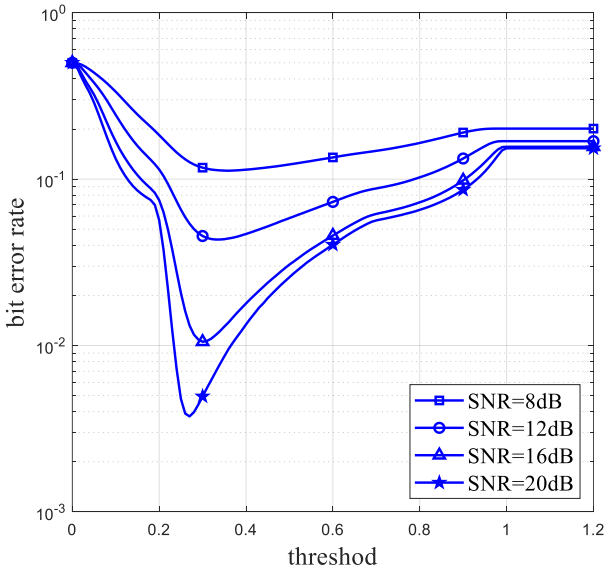

Figure 5.4: BER against blanking threshold under IN (ϵ = 0.04)

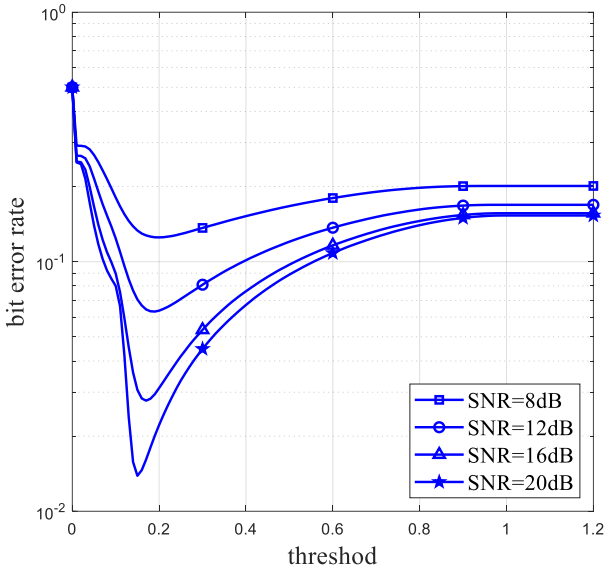

Figure 5.5: BER against clipping threshold under IN (ϵ = 0.04)

5.3 Threshold Values Selection

The main core of any nonlinear filter is selecting its threshold value which controls the alteration process of signal samples. When the amplitude of a signal sample overrides this threshold, it will be either snipped by clipping or set to zero by blanking.

It is important to beware when minimizing BER at the receiver to keep on the original signal samples and only modify the samples affected by IN. This is verified through a careful threshold selection by the nonlinear filter. It should be taken into consideration neither to choose very small values of T_c or T_b where most of the received samples will be clipped or blanked which innovates an output signal with many flaws. Also, nor to choose the very large values which leads the filters into averting the whole signal including the deteriorated impulsive ones. Accordingly, the accurate selection for clipping and blanking thresholds reinforces the correct detection of IN and enhances the nonlinear units' operations.

In this study, we employed blanking and clipping filters for reducing the effect of IN on mmWave communications systems. Since the existing thresholding mechanisms are mostly developed for microwave communications systems, they are not suitable for mmWave communications systems in their original form. In addition, the use of fixed threshold value does not promise optimal performance at different noise levels. Thus, a novel thresholding mechanism for IN mitigation is suggested and mathematical expressions for optimum threshold selection are obtained for the preprocessor filters. The optimal thresholding expression is derived by investigating the system performance under different scenarios to minimize the BER of the system. The effect of IN on BER and spectral efficiency of the system is examined with the use of optimal threshold values at the filters. As well as minimizing the BER, use of the proposed thresholding mechanism also maximizes the spectral efficiency of the system under IN.

The comparative values of SNR and the Effective SNR (SNRE), defined as the average signal power over the average total noise power at different ϵ, are given in Table 5.1 when SINR equals to -10 dB. As clearly seen from Table 5.1, the presence of the impulsive components in the noise reduces SNRE at the receiver significantly. Hence an effective mechanism to compensate for the effect of IN component and increasing the effective SNR is needed.

Figs. 5.6 and 5.7 present how the optimal threshold values for blanking and clipping change with SNRE at different ϵ values respectively. An analytical expression for optimal threshold is obtained by fitting the data collected, as presented in Figs. 5.6 and 5.7, to a polynomial surface of degree 2 in SNRE and ϵ as:

$$T_o(\gamma_e, \epsilon) = a_0 + a_1\gamma_e + a_2\epsilon + a_3\gamma_e^2 + a_4\gamma_e\epsilon + a_5\epsilon^2 \quad (5.1)$$

where a_o=0.8279, a_1=0.002594, a_2=0.6283, a_3=-0.002743, a_4=-2.943, a_5=-59.95 for optimal threshold for blanking filter (T_{bo}) and a_o=0.5525, a_1=-0.01492, a_2=-3.886, a_3=-0.0007977, a_4=-1.169, a_5=4.239 for the optimal threshold of clipping filter (T_{co}). γ_e is used to represent SNRE in (5.1) and can be calculated as:

$$\gamma_e = 10\ \log_{10}\left(\frac{P_{av}}{\sigma_e}\right) \quad (5.2)$$

where P_{av} stands for average received power, and $\sigma_e = (1-\epsilon)\sigma_w^2 + \epsilon\sigma_z^2$.

Table 5.1: SNRE versus SNR at different ϵ values

SNR, dB	SNRE, dB					
	ϵ=0.00	ϵ =0.01	ϵ =0.02	ϵ =0.03	ϵ =0.04	ϵ =0.05
-2.00	-2.00	-2.22	-2.44	-2.64	-2.84	-3.02
0.00	0.00	-0.37	-0.72	-1.04	-1.34	-1.61
2.00	2.00	1.40	0.87	0.40	-0.02	-0.41
4.00	4.00	3.06	2.29	1.64	1.07	0.56
6.00	6.00	4.58	3.51	2.65	1.93	1.32
8.00	8.00	5.90	4.49	3.43	2.58	1.87
10.00	10.00	7.01	5.26	4.01	3.05	2.25
12.00	12.00	7.89	5.82	4.42	3.37	2.52
14.00	14.00	8.56	6.22	4.70	3.58	2.69
16.00	16.00	9.04	6.49	4.89	3.73	2.81
18.00	18.00	9.37	6.66	5.01	3.82	2.88
20.00	20.00	9.59	6.78	5.09	3.88	2.93
22.00	22.00	9.74	6.86	5.14	3.91	2.96

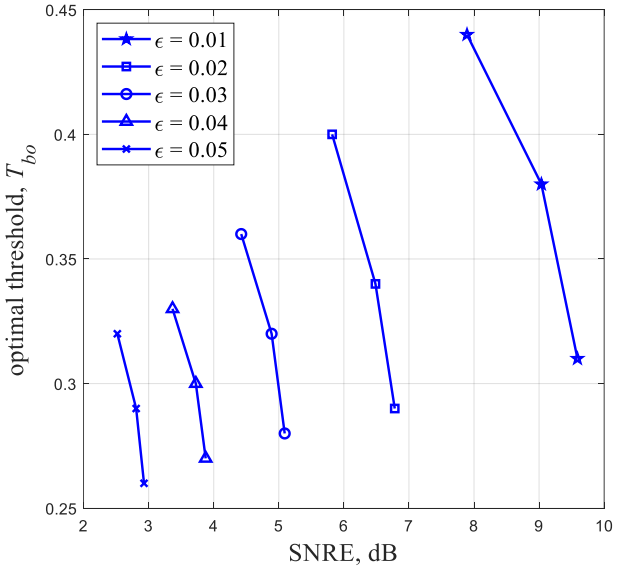

Figure 5.6: Optimal blanking threshold versus SNRE

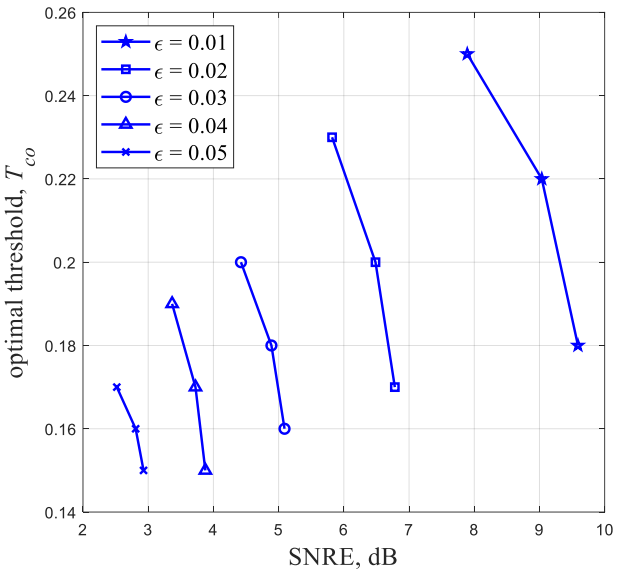

Figure 5.7: Optimal clipping threshold versus SNRE

5.3.1 Threshold Values Selection for Hybrid Filter

Based on the aforementioned, the hybrid preprocessor is distinguished by two thresholds T_1 and T_2 which are associated together through $T_2 = KT_1$. In fact, the performance of the preprocessor is sensitive not only to threshold T_1 but also to the proportionality constant K. The clipping threshold is set to optimal value of the

clipping threshold, T_{co}, defined by (5.1). Therefore, in this section, the adequacy of the hybrid filter is improved by optimizing the proportionality constant $K = T_2/T_{oc}$.

Figure 5.8 illustrates how BER alters with different values K under $\epsilon = 0.02$. Taking into consideration different values of SNR, the hybrid system can obtain better performance than clipping and blanking. The figure shows that the best BER values are obtained when K is set between 1.7 and 2.

It is encouraging to realize that the hybrid filter still fares much better than clipping and blanking filters in achieving better BER through Figure 5.9, which depicts BER versus different values of K under $\epsilon = 0.04$. From this figure, it is inferred that best BER improvements are obtained when K alters between 1.8 and 2.2. Therefore, for the hybrid filter, T_1 is set to the optimal threshold value T_{oc} and T_2 is set to $1.9T_{oc}$.

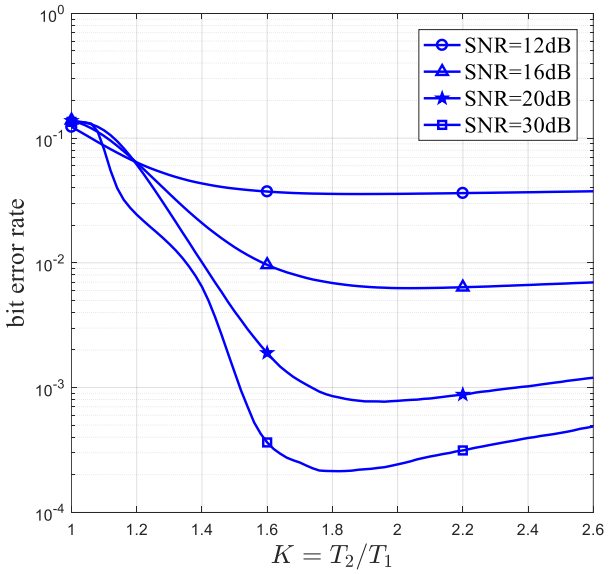

Figure 5.8: BER against $K = T_2/T_1$ under IN ($\epsilon = 0.02$)

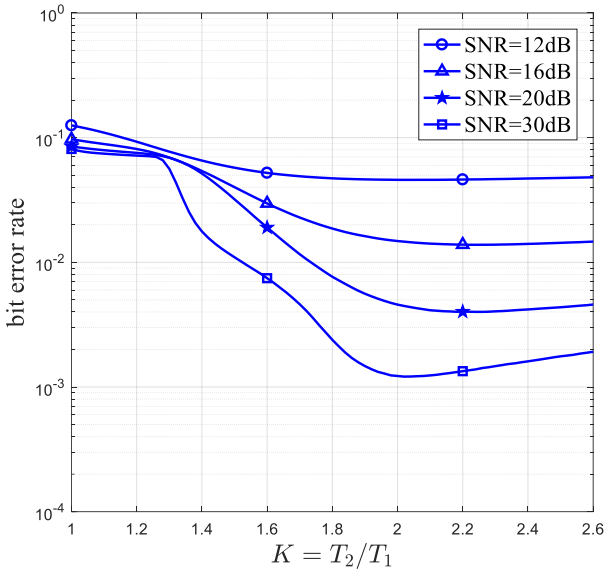

Figure 5.9: BER against $K = T_2/T_1$ under IN (ϵ = 0.04)

5.4 Performance Analysis of BER

At the front end of the receiver side where clipping, blanking and hybrid filters are positioned to perform IN suppression, their potential to boost the minimization in BER should be verified. For all the simulations presented in this and the following sections, the optimal threshold values for blanking and clipping filters are obtained from (5.1).

Based on the simulation parameters that have been mentioned in the beginning of this chapter, the used signaling is 16-QAM scheme. The performance is also tested for 2-QAM and 4-QAM signaling for some specific cases. While the higher-order schemes can attain much faster data rates and higher levels of spectral efficiency for the wireless system, they are considerably more susceptible to noise and interference.

5.4.1 Performance Analysis of BER for 2-QAM (BPSK)

It is observed in Figure 5.10 that the system with hybrid filter gives best results when M = 2. The same scenario is repeated for ϵ = 0.04. Figure 5.11 portrays that the

results obtained with the use of hybrid filter outperforms the results obtained with other two filters. The use of clipping filter gives the worst results in all cases. It is noticeable from the results that a BER floor occurs at large SNR values.

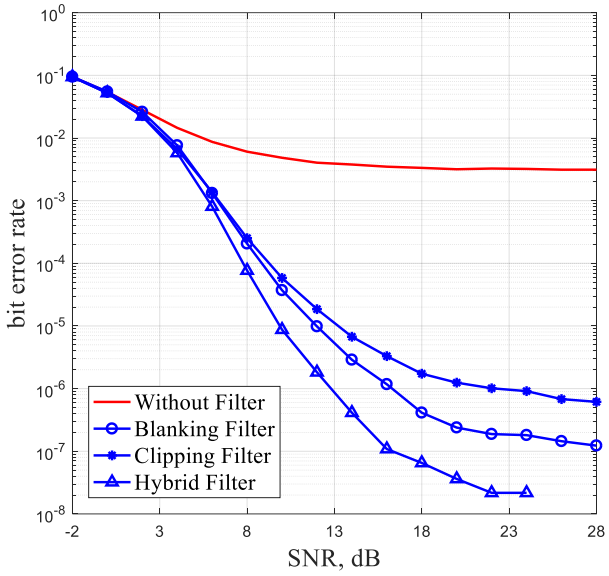

Figure 5.10: BER of mmWave system with and without clipping, blanking and hybrid filters versus SNR under IN (ϵ = 0.02) for 2-QAM (BPSK)

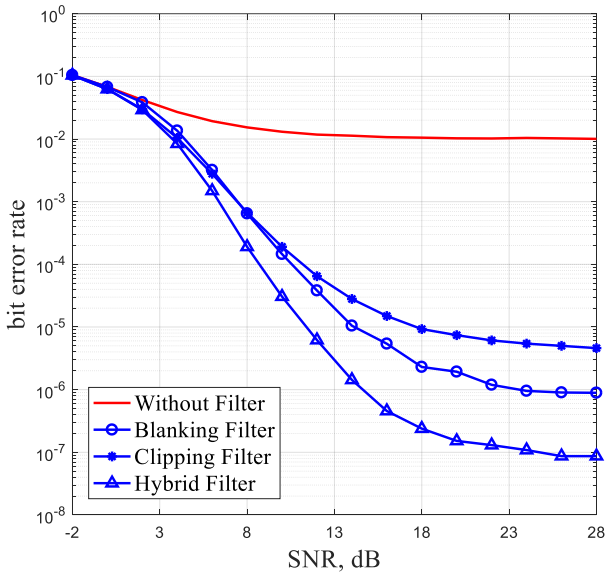

Figure 5.11: BER of mmWave system with and without clipping, blanking and hybrid filters versus SNR under IN (ϵ = 0.04) for 2-QAM (BPSK)

5.4.2 Performance Analysis of BER for 4-QAM (QPSK)

Figure 5.12 presents BER versus SNR for the three filters under $\epsilon = 0.02$ and $M = 4$. All nonlinear filters operate effectively in reducing BER, nevertheless, the hybrid filter exceeds clipping and blanking in attaining 2×10^{-6} of BER followed by a blanking filter. Identically, the performance of preprocessors is a bit changed in the more intense impulsive case when $\epsilon = 0.04$ as illustrated by Figure 5.13. It can be easily observed from this figure that the hybrid filter still superintends over clipping and blanking filters and gains a BER of 9×10^{-6}. A BER floor can be observed from the simulating results especially at high SNR values, this is expected since there is a constant IN of -10 dB which does not allow SNRE value to increase and keeps it constant after a certain SNR.

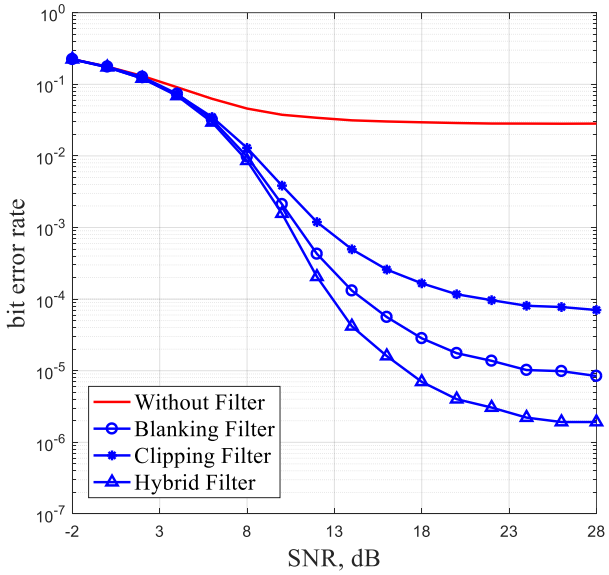

Figure 5.12: BER of mmWave system with and without clipping, blanking and hybrid filters versus SNR under IN ($\epsilon = 0.02$) for 4-QAM (QPSK)

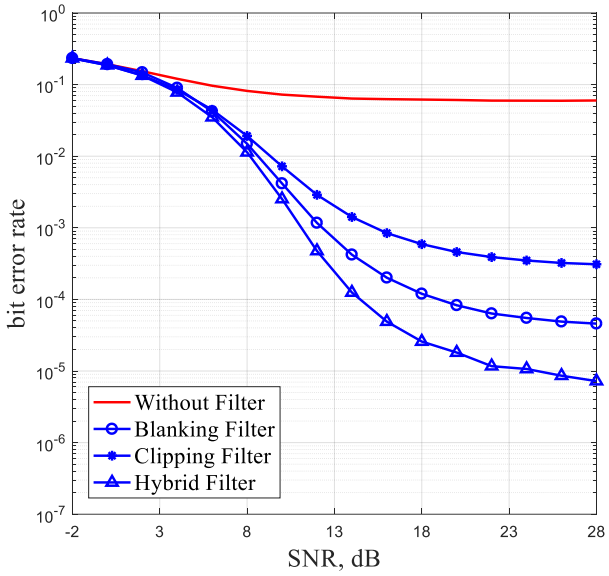

Figure 5.13: BER of mmWave system with and without clipping, blanking and hybrid filters versus SNR under IN (ϵ = 0.04) for 4-QAM (QPSK)

5.4.3 Performance Analysis of BER for 16-QAM

Figure 5.14 and Figure 5.15 display a comparison between the three filters used for IN mitigation in mmWave system. It can be notified from Figure 5.14 that for ϵ = 0.02, hybrid is slightly approaching to blanking filter performance up to SNR=18.5 dB, beyond, it overrides blanking and achieves a BER of 3×10^{-4}. While, blanking outperforms clipping for SNR values between 6 dB and 22 dB with a BER enhancement of 7×10^{-4}. However, in the more intense impulsive environment at ϵ = 0.04, the performance of all preprocessors somewhat back off, yet still, gain improved BER results as illustrated by Figure 5.15. It is clearly shown in this figure that in the range of 12 to 24 dB SNR, blanking filter outperforms clipping and hybrid units. Nevertheless, on the further side after 24 dB, hybrid surpasses clipping and blanking and obtains the best BER of 1×10^{-3} while blanking filter gains 3×10^{-3}. Base on the results, we conclude that, system shows better BER performance with hybrid filter only for high SNR values. However the performance obtained with the

blanking filter slightly outperforms the performance obtained with the use of hybrid filter at lower SNR values.

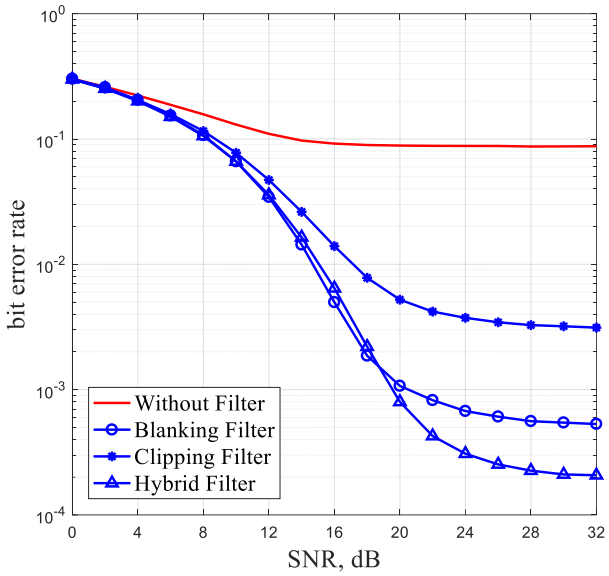

Figure 5.14: BER of mmWave system with and without clipping, blanking and hybrid filters versus SNR under IN (ϵ = 0.02) for 16-QAM

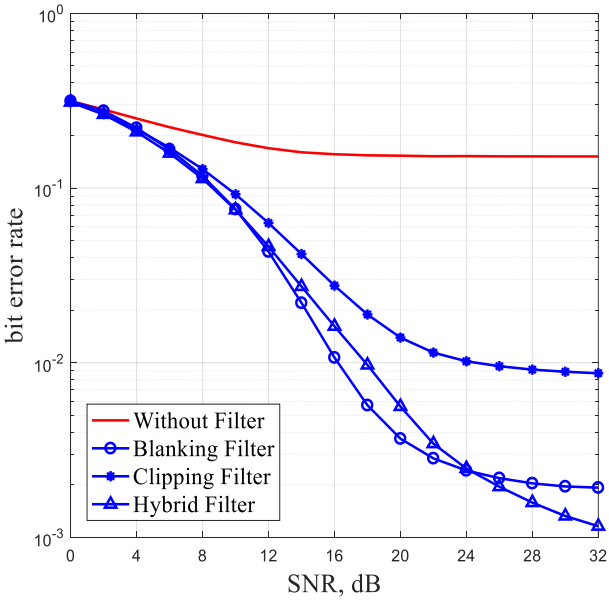

Figure 5.15: BER of mmWave system with and without clipping, blanking and hybrid filters versus SNR under IN (ϵ = 0.04) for 16-QAM

The relation between BER and SNRE for the three filters is examined through Figure 5.16. According to Table 5.1, it is worth mentioning that starting at SNR=12 dB and above, the value of SNRE remains constant around 6.8 dB at ϵ = 0.02 and SINR=-10 dB. The sequence of the nonlinear units in achieving the best result is somehow a replica for the previous approaches as depicted in the figure. Clipping did the least performance in comparison with blanking which almost converges the efficacy of the hybrid filter. Hybrid filter could obtain a BER of 8.5×10^{-4} while the blanking filter succeeds to achieve a BER of 1×10^{-3}.

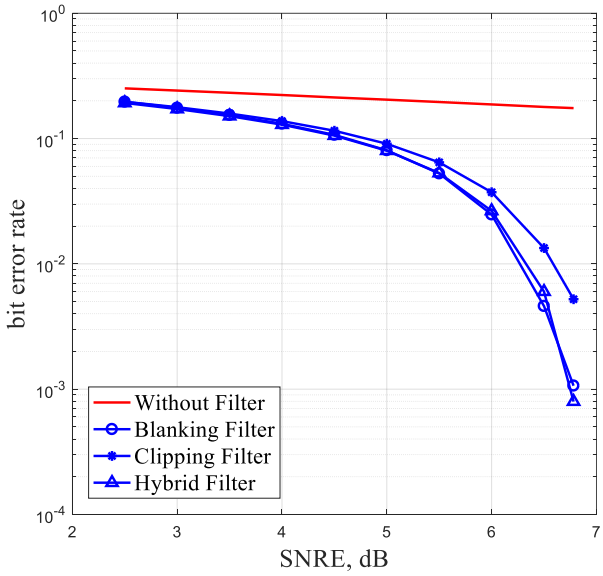

Figure 5.16: BER of mmWave system with and without clipping, blanking and hybrid filters versus SNRE under IN (ϵ = 0.02) for 16-QAM

Intuitively, it can be deduced that the clipping filter performs the least among all filters even though it works effectively in suppressing the effect of IN. Among the nonlinear preprocessors, the hybrid filter keeps on its supremacy over clipping and blanking in enhancing system performance at different impulsive environments and variant conditions and schemes. Nevertheless, at high SNR values it presents slightly better performance, thus it will not be used for further simulations.

5.5 Performance Analysis of Spectral Efficiency

In this section, the impact of IN and the role of utilizing clipping and blanking filters in improving the spectral efficiency of the system are investigated. The spectral efficiency curves are obtained from the following rate expression:

$$R = log_2 \left| \mathbf{I}_{N_s} + \frac{P_{\text{av}}}{\sigma_e N_S} (\mathbf{W}_{\text{RF}} \mathbf{W}_{\text{BB}})^H \mathbf{H} \mathbf{F}_{\text{RF}} \mathbf{F}_{\text{BB}} \times \mathbf{F}_{\text{BB}}^H \mathbf{R}^{-1} \mathbf{F}_{\text{BB}}^H \mathbf{H}^H (\mathbf{W}_{\text{RF}} \mathbf{W}_{\text{BB}}) \right| \quad (5.3)$$

where, for a matrix $|\ \ |$ represents the determinant.

The severe effect of IN on spectral efficiency of mmWave system without implementing clipping and blanking filters is apparent in Figure 5.17 at ϵ = 0.02 and 0.04.

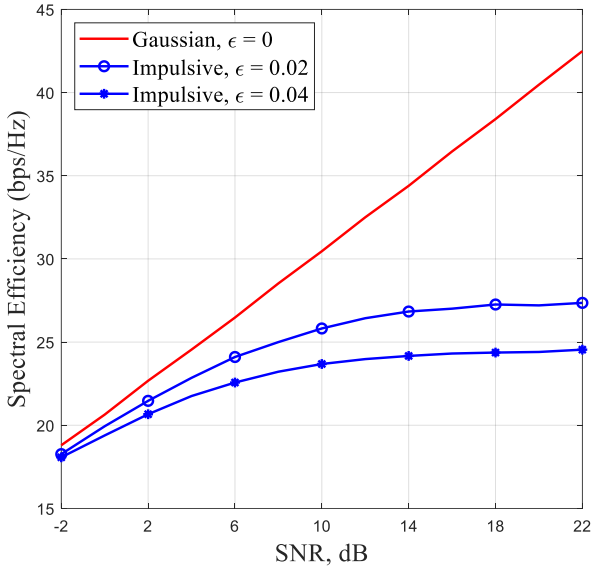

Figure 5.17: Spectral efficiency of mmWave system versus SNR under Gaussian and IN

Notwithstanding, it can be seen that the simulation results for applying clipping and blanking filters submit a spectral efficiency improvement. Figure 5.18 depicts the total achievable spectral efficiency under $\epsilon = 0.02$ when blanking and clipping are exploited. Clearly, spectral efficiency remains the same and very tight for both filters in the low and moderate SNR range (SNR < 10 dB). Furthermore, when SNR > 10 dB, it can be observed that the total achievable spectral efficiency for blanking and clipping converges to a saturated value. While in Figure 5.19, the performance of spectral efficiency is reduced for clipping and blanking under a severe impulsive environment when $\epsilon = 0.04$. Nevertheless, blanking surpasses clipping at $\epsilon = 0.02$ and $\epsilon = 0.04$.

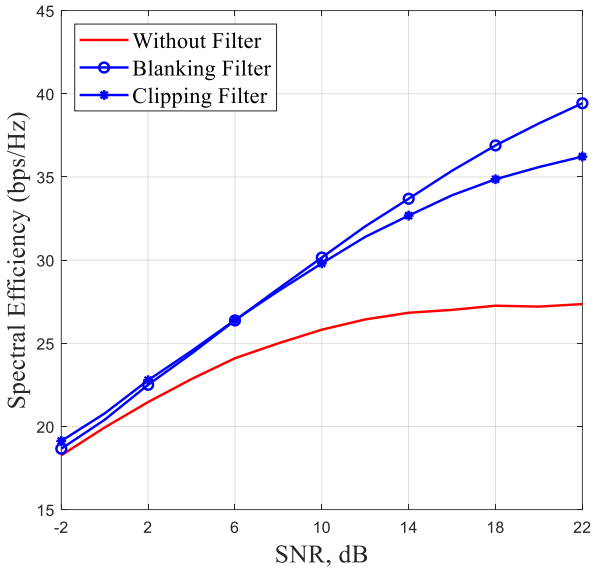

Figure 5.18: Spectral efficiency of mmWave system versus SNR under IN (ϵ = 0.02) with and without blanking and clipping filters

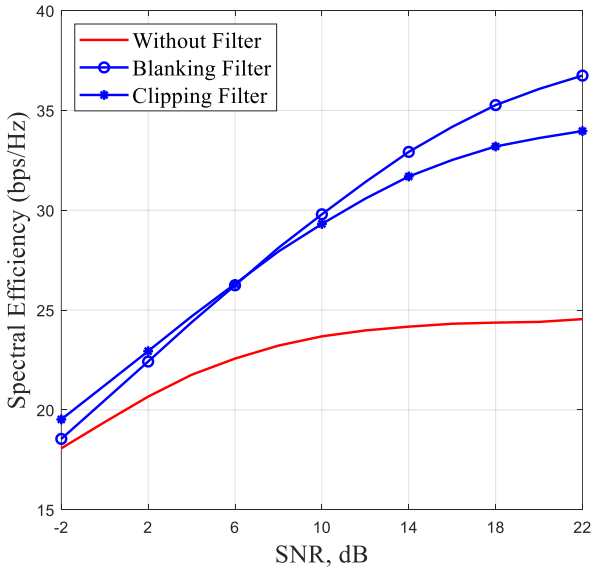

Figure 5.19: Spectral efficiency of mmWave system versus SNR under IN (ϵ = 0.04) with and without blanking and clipping filters

Meanwhile in Figure 5.20, the performance of spectral efficiency of the system is illustrated through the system without filters and when using them for variant values at 10 dB and 20 dB of SNR. It is shown that spectral efficiency grows with the increment in SNR where at 20 dB, it is improved for clipping and blanking than at 10

dB. The filters tend to manifest improvement in spectral efficiency, and as typical, the blanking filter outperforms.

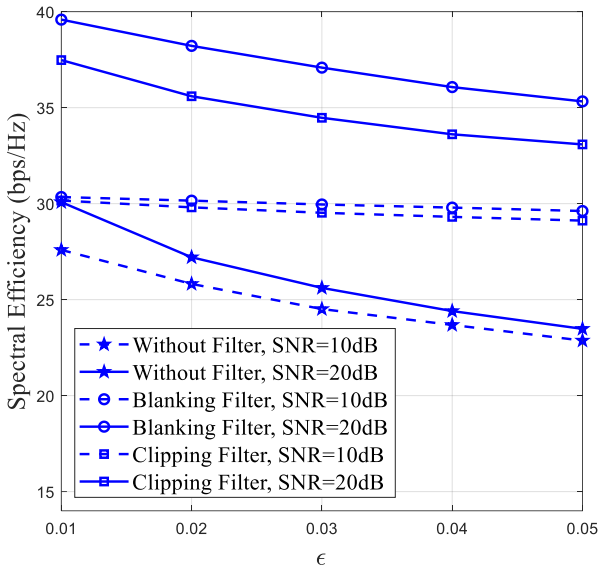

Figure. 5.20: Spectral efficiency of mmWave system versus ϵ under IN with and without blanking and clipping filters

Chapter 6

CONCLUSION AND FUTURE WORK

In spite of its huge scientific researches during the last two decades, there is a lack in mmWave system research, particularly in the field of IN studies. Therefore, there is an urgent need to investigate this rare subject, narrowing the gap that is ignored by the researchers. The present study is conducted to suppress the effect of IN in the field of mmWave system.

6.1 Conclusion

This study aims at detecting the existence of IN in mmWave technology, revealing the performance of the nonlinear preprocessors when applied for both Gaussian noise and IN, examining the function of the outperforming of the nonlinear preprocessors in mitigating IN in mmWave system, proposing algorithms for the conducted nonlinear preprocessors to improve the performance of the mmWave system in an impulsive environment, and finally developing a method to get the optimum thresholds for the proposed preprocessors. For attaining the objectives, clipping, blanking and hybrid preprocessors were exploited. They are considered the simplest, the most effective techniques and a straightforward way to suppress the adverse impact of IN. Technically, they are widely used to limit and null the amplitudes of signal samples when exceeding the higher impulsive amplitudes without influencing the phases.

This thesis highlighted the main features of mmWave system and the challenges facing this technology accompanied by a focus on IN suppression through the nonlinear preprocessors over such system. Chapter 2 deliberated about the characteristics of mmWave system and its impairments such as blockage, diffraction, atmospheric absorption, and noises. As a prosperous partition of 5G technology, mmWave system overrides many techniques and platforms through the distinguished mannerism of its own high frequencies in the cellular network. Different architectures and hierarchies which explained many configurations for the optimum wave propagation through mmWave system are outlined in this chapter.

Chapter 3 briefly introduced the influence of noises on mmWave system. Nevertheless, it mightily debated IN, its features, attitude and models. In addition, this chapter revealed the impact of IN on high frequencies over radar, beamforming, electrical substations, optical fiber, and global positioning systems. The conventional IN mitigation techniques are exposed and compared in chapter 4 such as blanking, clipping and hybrid filters. However, new algorithms for blanking, clipping and hybrid preprocessors were adapted for mmWave system in chapter 4 to combat the impulsive effect and gain better BER and SNR. The nonlinear preprocessor unit was placed at the front end of the receiver of the mmWave system model to best result attained. Chapter 5 examined the proposed algorithms and optimized the blanking and clipping thresholds in such a way to maximize the output SNR performance. The chapter also revealed the decreased impulsive impact when filters were exploited. Further, the comparisons between clipping, blanking and hybrid filters to mitigate IN are illustrated through simulations, led by the hybrid unit. Hybrid showed its best performance over clipping and blanking in a moderate impulsive environment at $\epsilon =$

0.02, while was less efficient in a heavier impulsive ambient but still outperformed the other two filters. At 20 dB of SNR, hybrid filter was the best choice to do the impulsive mitigation process by gaining 8.5×10^{-4} of BER versus 9.9×10^{-4} for blanking, while clipping achieved a BER of 6.3×10^{-3}. For all cases, hybrid filter kept on gaining lower BER over clipping and blanking and this makes hybrid the favorable filter to do IN mitigation function under the current system conditions. For some specific cases, a comparison was set between 2-QAM, 4-QAM, and 16-QAM schemes to examine the performance of nonlinear preprocessors in mitigating IN. The system performance was at the utmost level when $M = 2$, and this is obviously due to the reason that the higher-order schemes are more susceptible to noise than the lower-order ones.

For the aforementioned different impulsive environments and variant conditions and schemes, it was found that clipping did the least efficacy while the hybrid unit gained supremacy. However, on the one hand, the performance of the hybrid unit is rising within the high SNR values, while on the other hand, for the low SNR values, blanking slightly surpassed the hybrid filter. Based on the simulation results, a BER floor can be observed particularly at high SNR values, this is owed to the constant value of SINR which forbade any increment in SNRE value after a certain SNR.

Meanwhile, IN suppressing was enhanced through applying the optimizing threshold techniques for all filters to attain better SNR and BER. Through analytical expressions, the optimal threshold values were obtained for both filters changing with SNRE at different ϵ values to maximize SNR performance. At the least impulsive case when $\epsilon = 0.01$, the best threshold value for clipping was 0.17 while it was 0.33 for blanking. On the other hand, at $\epsilon = 0.05$, it was 0.18 for clipping and

0.31 for blanking. The adequacy of the hybrid filter was improved by committing the clipping optimal threshold and optimizing the proportionality constant. For variant impulsive ambiences, it was found that hybrid filter outperformed clipping and blanking when the proportionality constant is adjusted between 1.7 and 2.2.

The spectral efficiency for mmWave system is investigated also under clipping and blanking filters. Blanking outperforms clipping by 4 bps/Hz in both impulsive environments at $\epsilon = 0.02$ and $\epsilon = 0.04$, however, the best achieved spectral efficiency was at $\epsilon = 0.2$ and 20 dB SNR. Moreover, it was observed that when SNR is beyond 10 dB value, the total achievable spectral efficiency for blanking and clipping converges to a saturated value.

Despite most of the thesis work was based on computer simulations and some analysis, the implementation that has been performed is being inspiring and suggestive. Besides, it could fill a bit of the gap that is ignored and left. Meanwhile, this thesis is looking to do at least a small contribution to the vast field of 5G.

6.2 Future Work

Under the light of study's procedures, findings and discussions, the following recommendations and suggestions are set up:

6.2.1 Recommendations

1. In chapter 4, the proposed algorithm presented for clipping, blanking and hybrid filters achieved a moderate performance to suppress IN effect in mmWave system. However, it would be worthwhile to improve it more to gain better SNR and BER values.

2. In chapter 5, Figs. 5.6 and 5.7 prop the optimized thresholds calculations for both clipping and blanking. Nevertheless, it will be more instructive to derive mathematical expressions for optimizing the clipping and blanking thresholds to be applicable for any identical system.
3. In chapter 5, the impact of IN was reduced through clipping, blanking and hybrid preprocessors practically by using MATLAB. It would be much improved if it is proved theoretically via mathematical equations.
4. Clipping, blanking and hybrid filters are concerned as IN mitigation techniques in chapter 5, however, this could be extended to more filters and algorithms for investigating their compatibility for mmWave system.

6.2.2 Suggestions

For the searching's importance in the field of mmWave, the researcher sets the following suggestions that could underpin and support the thorough and logical searching in this aspect: a) increasing the concern of IN impact in the researches of 5G technology at all levels. b) developing algorithms and techniques for investigating the effect of IN; and c) executing several practical experiments to implement the proposed techniques in this thesis, which will be a good indication of their compatibility with the real-life.

REFERENCES

[1] Rappaport, T. S. (1996). *Wireless communications: principles and practice* (Vol. 2). New Jersey: prentice hall PTR.

[2] Goldsmith, A. (2005). *Wireless communications*. Cambridge university press.

[3] Osseiran, A., Monserrat, J. F., & Marsch, P. (Eds.). (2016). *5G mobile and wireless communications technology*. Cambridge University Press.

[4] Dahlman, E., Parkvall, S., & Skold, J. (2018). *5G NR: The next generation wireless access technology*. Academic Press.

[5] E. Çatak and L. Durak-Ata, *Towards 5G Wireless Networks a Physical Layer Perspective, Chapter Two*, ExLi4EvA, 2016. From Bizaki, H. K. (Ed.). (2016). *Towards 5G Wireless Networks: A Physical Layer Perspective*. BoD–Books on Demand.

[6] Fizza, M., & Shah, M. A. (2016). 5G Technology: An Overview of Applications, Prospects, Challenges and Beyond. *Proceedings Appeared on IOARP Digital Library*.

[7] Roh, W., Seol, J. Y., Park, J., Lee, B., Lee, J., Kim, Y. & Aryanfar, F. (2014). Millimeter-wave beamforming as an enabling technology for 5G cellular communications: Theoretical feasibility and prototype results. *IEEE communications magazine*, *52*(2), 106-113.

[8] Weiler, R. J., Peter, M., Keusgen, W., Calvanese-Strinati, E., De Domenico, A., Filippini, I. & Haustein, T. (2014, June). Enabling 5G backhaul and access with millimeter-waves. In*2014 European Conference on Networks and Communications (EuCNC)* (pp. 1-5). IEEE.

[9] Andrews, J. G., Bai, T., Kulkarni, M. N., Alkhateeb, A., Gupta, A. K., & Heath, R. W. (2016). Modeling and analyzing millimeter wave cellular systems. *IEEE Transactions on Communications*, *65*(1), 403-430.

[10] Rappaport, T. S., Xing, Y., MacCartney, G. R., Molisch, A. F., Mellios, E., & Zhang, J. (2017). Overview of millimeter wave communications for fifth-generation (5G) wireless networks—with a focus on propagation models. *IEEE Transactions on Antennas and Propagation*, *65*(12), 6213-6230.

[11] Yu, X., Shen, J. C., Zhang, J., & Letaief, K. B. (2016). Alternating minimization algorithms for hybrid precoding in millimeter wave MIMO systems. *IEEE Journal of Selected Topics in Signal Processing*, *10*(3), 485-500.

[12] Rappaport, T. S., Sun, S., Mayzus, R., Zhao, H., Azar, Y., Wang, K. & Gutierrez, F. (2013). Millimeter wave mobile communications for 5G cellular: It will work. *IEEE access*, *1*, 335-349.

[13] Wang, P., Li, Y., Song, L., & Vucetic, B. (2015). Multi-gigabit millimeter wave wireless communications for 5G: From fixed access to cellular networks. *IEEE Communications Magazine*, *53*(1), 168-178.

[14] Rappaport, T. S., Heath Jr, R. W., Daniels, R. C., & Murdock, J. N. (2014). *Millimeter wave wireless communications*. Pearson Education.

[15] Abdin, M. M., Joel, W., Johnson, D., & Weller, T. M. (2017, April). A system and technology perspective on future 5G mm-wave communication systems. In *2017 IEEE 18th Wireless and Microwave Technology Conference (WAMICON)* (pp. 1-6). IEEE.

[16] Feng, W., Li, Y., Jin, D., Su, L., & Chen, S. (2016). Millimeter-wave backhaul for 5G networks: Challenges and solutions. *Sensors*, *16*(6), 892.

[17] Huang, K. C., & Wang, Z. (2011). *Millimeter wave communication systems* (Vol. 29). John Wiley & Sons.

[18] Wostencroft, R. D. & Burton, W. B. (1987). Millimeter and Submillimeter Astronomy: Millimeter and Submillimtere Astronomy and Cosmology: What Everyone Really Needs to Know (by M. Longair), vol. 147.

[19] Olver, A. D. (1989, February). Millimeter wave systems—past, present and future. In *IEE Proceedings F (Radar and Signal Processing)* (Vol. 136, No. 1, pp. 35-52). IET Digital Library.

[20] Skolnik, M. I. (1970). *Millimeter and submillimeter wave applications* (No. NRL-MR-2159). NAVAL RESEARCH LAB WASHINGTON DC.

[21] R. Belcher, “Extremely High Frequency (EHF) Low Probability of Intercept (LPI) Communication Applications,” Naval Postgraduate School, Master thesis, 1990, USA.

[22] Mumtaz, S., Rodriguez, J., & Dai, L. (2016). *MmWave Massive MIMO: A Paradigm for 5G*. Academic Press.

[23] Pi, Z., & Khan, F. (2011). An introduction to millimeter-wave mobile broadband systems. *IEEE communications magazine*, *49*(6), 101-107.

[24] Marcus, M., & Pattan, B. (2005). Millimeter wave propagation: spectrum management implications. *IEEE Microwave Magazine*, *6*(2), 54-62.

[25] Kang, M. S., Kim, B. S., Kim, K. S., Byun, W. J., Song, M. S., & Oh, S. H. (2010, February). Wireless PtP system in E-band for gigabit ethernet. In *2010 The 12th International Conference on Advanced Communication Technology (ICACT)* (Vol. 1, pp. 733-736). IEEE.

[26] Wei, L., Hu, R. Q., Qian, Y., & Wu, G. (2014). Key elements to enable millimeter wave communications for 5G wireless systems. *IEEE Wireless Communications*, *21*(6), 136-143.

[27] Hemadeh, I. A., Satyanarayana, K., El-Hajjar, M., & Hanzo, L. (2017). Millimeter-wave communications: Physical channel models, design considerations, antenna constructions, and link-budget. *IEEE Communications Surveys & Tutorials*, *20*(2), 870-913.

[28] M. Peter, “Measurement, Characterization and Modeling of Millimeter Wave Channels: from 60 GHz to 5G,” PhD Dissertation, Technical University of Berlin, 2017.

[29] Hueber, G., & Niknejad, A. M. (Eds.). (2019). *Millimeter-wave Circuits for 5G and Radar*. Cambridge University Press.

[30] F. L. Luo and C. Zhang, *Signal Processing for 5G: Algorithms and Implementations*, 1st Edition, IEEE Press, John Wiley & Sons Ltd., 2016. UK.

[31] Allen, B., & Ghavami, M. (2005). *Adaptive array systems: fundamentals and applications*. John Wiley & Sons.

[32] Naidu, P. S. (2009). *Sensor array signal processing*. CRC press.

[33] Busari, S. A., Huq, K. M. S., Mumtaz, S., Dai, L., & Rodriguez, J. (2017). Millimeter-wave massive MIMO communication for future wireless systems: A survey. *IEEE Communications Surveys & Tutorials*, *20*(2), 836-869.

[34] Fan, D., Gao, F., Liu, Y., Deng, Y., Wang, G., Zhong, Z., & Nallanathan, A. (2018). Angle Domain Channel Estimation in Hybrid Millimeter Wave Massive MIMO Systems. *IEEE Transactions on Wireless Communications*, *17*(12), 8165-8179.

[35] Zhou, Z., Fang, J., Yang, L., Li, H., Chen, Z., & Li, S. (2016). Channel estimation for millimeter-wave multiuser MIMO systems via PARAFAC

decomposition. *IEEE Transactions on Wireless Communications*, *15*(11), 7501-7516.

[36] Vaseghi, S. V. (2008). *Advanced digital signal processing and noise reduction*. John Wiley & Sons.

[37] R. Ziemer, W. Tranter, *Principles of Communications: Systems, Modulation and Noise*, 7th Edition, John Wiley & Sons, Inc., USA, 2015.

[38] Baudin, P. (2014). *Wireless Transceiver Architecture: Bridging RF and Digital Communications*. John Wiley & Sons.

[39] Rangan, S., Rappaport, T. S., & Erkip, E. (2014). Millimeter wave cellular wireless networks: Potentials and challenges.*arXiv preprint arXiv: 1401.2560*.

[40] James, J., Shen, P., Nkansah, A., Liang, X., & Gomes, N. J. (2010). Nonlinearity and noise effects in multi-level signal millimeter-wave over fiber transmission using single and dual wavelength modulation. *IEEE Transactions on Microwave Theory and Techniques*, *58*(11), 3189-3198.

[41] A. Abdul Waheed, "Mitigation of Phase Noise at Millimeter-Wave Frequencies for Wireless Personal Area Network Applications," *Master Thesis*, University of Massachusetts Amherst, Electrical and Computer Engineering, 2008.

[42] Grimwood, N., Dean, T., & Goldsmith, A. (2018, October). Robustness of FDM-FDCP Modulation to Phase Noise in Millimeter Wave Systems. In *2018*

52nd Asilomar Conference on Signals, Systems, and Computers (pp. 264-268). IEEE.

[43] Va, V., Choi, J., Shimizu, T., Bansal, G., & Heath, R. W. (2018). Impact of measurement noise on millimeter wave beam alignment using beam subsets. *IEEE Wireless Communications Letters*, *7*(5), 784-787.

[44] Marcus, M., & Pattan, B. (2005). Millimeter wave propagation: spectrum management implications. *IEEE Microwave Magazine*, *6*(2), 54-62.

[45] Niknam, S., Mehrpouyan, H., & Natarajan, B. (2017, September). A spatial-spectral interference model for millimeter wave 5G applications. In *2017 IEEE 86th Vehicular Technology Conference (VTC-Fall)* (pp. 1-5). IEEE.

[46] Saleh, T. S. S. M. (2012). *Receiver design for signals in non-Gaussian noise: applications to symmetric alpha-stable and Middleton's class-A noise models* (Doctoral dissertation, Carleton University).

[47] Parsons, J. D. & Gardiner, J. G. (1989). *Mobile communication systems*. Halsted Press, John Wiley & Sons, Inc., USA.

[48] Gomez, J. (2017). A Survey on Impulsive Noise Modeling. *Revista Telematica*. 16(1), 101-113.

[49] Agba, B. L., Sacuto, F., Au, M., Labeau, F., & Gagnon, F. (2019). *Wireless Communications for Power Substations: RF Characterization and Modeling*. Springer International Publishing.

[50] Gulati, K., Chopra, A., Heath Jr, R. W., Evans, B. L., Tinsley, K. R., & Lin, X. E. (2008, December). MIMO receiver design in the presence of radio frequency interference. In *IEEE GLOBECOM 2008-2008 IEEE Global Telecommunications Conference* (pp. 1-5). IEEE.

[51] Plataniotis, K., & Hatzinakos, D. (2017). Gaussian Mixtures and Their Application to Signal Processing. In S. Stergiopoulos (Ed.), *Advanced signal processing handbook: theory and implementation for radar, sonar, and medical imaging real time systems* (pp. 3-1 – 3-32)*:* Boca Raton, Florida: CRC press.

[52] RECOMMENDATION ITU-R P.372-8, Radio Noise.

[53] Shan, Q., Glover, I. A., Atkinson, R. C., Bhatti, S. A., Portugues, I. E., Moore, P. J., ... & De Souza, B. A. (2011). Estimation of impulsive noise in an electricity substation. *IEEE Transactions on Electromagnetic Compatibility*, *53*(3), 653-663.

[54] Liu, L., & Amin, M. G. (2008). Performance analysis of GPS receivers in non-Gaussian noise incorporating precorrelation filter and sampling rate. *IEEE Transactions on Signal Processing*, *56*(3), 990-1004.

[55] Pham, K., Conradi, J., Cormack, G., Thomas, B., & Anderson, C. W. (1995). Impact of noise and nonlinear distortion due to clipping on the BER performance of a 64-QAM signal in hybrid AM-VSB/QAM optical fiber transmission system. *Journal of lightwave technology*, *13*(11), 2197-2201.

[56] Maeda, K., Nakata, H., & Fujito, K. (1993). Analysis of BER of 16QAM signal in AM/16QAM hybrid optical transmission system. *Electronics Letters*, *29*(7), 640-642.

[57] Badarneh, O. S., & Almehmadi, F. S. (2019). The effects of different noise types and mobility on error rate of digital modulation schemes over millimeter-wave Weibull fading channels. *Wireless Networks*, *25*(5), 2259-2268.

[58] Keckler, A. D., Stadelman, D. L., & Weiner, D. D. (1997, May). Non-Gaussian clutter modeling and application to radar target detection. In *Proceedings of the 1997 IEEE National Radar Conference* (pp. 240-245). IEEE.

[59] Sujuan, F., Wugao, L., & Dejun, Z. (1996, October). Modeling and simulation of non-Gaussian correlated clutter. In *Proceedings of International Radar Conference* (pp. 195-199). IEEE.

[60] Tsakalides, P., & Nikias, C. L. (1997, April). A new model for non-Rayleigh clutter: Space-time adaptive processing in stable impulsive interference. In *1997 IEEE International Conference on Acoustics, Speech, and Signal Processing* (Vol. 5, pp. 3517-3520). IEEE.

[61] Katkovnik, V. (2000). A new concept of adaptive beamforming for moving sources and impulse noise environment. *Signal processing*, *80*(9), 1863-1882.

[62] Sarabandi, K., Li, E. S., & Nashashibi, A. (1997). Modeling and measurements of scattering from road surfaces at millimeter-wave frequencies. *IEEE Transactions on Antennas and Propagation*, *45*(11), 1679-1688.

[63] Lee, M. S., Katkovnik, V., & Kim, Y. H. (2004). Robust approximate median beamforming for phased array radar with antenna switching. *Signal processing*, *84*(9), 1667-1675.

[64] Tian, Q., Qiu, T., Cai, R., & Ma, J. (2020). A Novel DOA Estimation for Distributed Sources in an Impulsive Noise Environment. *IEEE Access*, *8*, 61405-61420.

[65] Tian, Q., Qiu, T., Ma, J., Li, J., & Li, R. (2018). A simplified DOA estimation method based on correntropy in the presence of impulsive noise. *IEEE Access*, *6*, 67010-67025.

[66] Silva, H. S., Alencar, M. S., Queiroz, W. J., Almeida, D. B., & Madeiro, F. (2018). Closed-Form Expression for the Bit Error Probability of the-QAM for a Channel Subjected to Impulsive Noise and Nakagami Fading. *Wireless Communications and Mobile Computing*, *2018*.

[67] Juwono, F. H., Guo, Q., Huang, D., & Wong, K. P. (2014). Deep clipping for impulsive noise mitigation in OFDM-based power-line communications. *IEEE Transactions on Power Delivery*, *29*(3), 1335-1343.

[68] Wang, X., Cao, C. Q., Zeng, X. D., Pan, Z., Cheng, Y. H., & Luo, L. (2017). A high-quality 120 GHz millimeter-wave generation without laser phase noise. *Journal of Modern Optics*, *64*(1), 46-51.

[69] Monje, R. R., Cooper, K. B., Dengler, R. J., Bouayadi, T. O. E., & Gonzalez-Ovejero, D. (2017, August). High T/R isolation and phase-noise suppression in millimeter wave FMCW radars.

[70] Futatsumori, S., Morioka, K., Kohmura, A., Miyazaki, N., & Yonemoto, N. (2018, September). Effects of Transmission-Signal Phase Noise on the Performance of an Optically-Connected 96 GHz Millimeter-Wave Radar System. In *2018 IEEE Conference on Antenna Measurements & Applications (CAMA)* (pp. 1-2). IEEE.

[71] Rebato, M., Mezzavilla, M., Rangan, S., Boccardi, F., & Zorzi, M. (2016, May). Understanding noise and interference regimes in 5G millimeter-wave cellular networks. In *European Wireless 2016; 22th European Wireless Conference* (pp. 1-5). VDE.

[72] Kang, T. W., Kim, J. H., Kang, N. W., & Kang, J. S. (2014, August). Developing a thermal noise measurement system in W-band. In *29th Conference*

on Precision Electromagnetic Measurements (CPEM 2014) (pp. 176-177). IEEE.

[73] Roufarshbaf, H., Madhow, U., & Rajagopal, S. (2014, December). OFDM-based analog multiband: A scalable design for indoor mm-wave wireless communication. In *2014 IEEE Global Communications Conference* (pp. 3267-3272). IEEE.

[74] Lim, W., Kwon, G., & Park, H. (2017). Interference mitigation using random antenna selection in millimeter wave beamforming system. *EURASIP Journal on Wireless Communications and Networking*, *2017*(1), 87.

[75] Hoefle, M., Penirschke, A., Cojocari, O., Amrhein, A., Decoopman, T., Piironen, P., & Jakoby, R. (2013, September). 1/f-noise prediction in millimeter wave detectors based on quasi vertical Schottky diodes. In *2013 38th International Conference on Infrared, Millimeter, and Terahertz Waves (IRMMW-THz)* (pp. 1-3). IEEE.

[76] Niu, Y., Li, Y., Jin, D., Su, L., & Vasilakos, A. V. (2015). A survey of millimeter wave communications (mmWave) for 5G: opportunities and challenges. *Wireless networks*, *21*(8), 2657-2676.

[77] Akdeniz, M. R., Liu, Y., Samimi, M. K., Sun, S., Rangan, S., Rappaport, T. S., & Erkip, E. (2014). Millimeter wave channel modeling and cellular capacity evaluation. *IEEE journal on selected areas in communications*, *32*(6), 1164-1179.

[78] Alkhateeb, A., Leus, G., & Heath, R. W. (2015). Limited feedback hybrid precoding for multi-user millimeter wave systems. *IEEE transactions on wireless communications*, *14*(11), 6481-6494.

[79] Yu, X., Shen, J. C., Zhang, J., & Letaief, K. B. (2016). Alternating minimization algorithms for hybrid precoding in millimeter wave MIMO systems. *IEEE Journal of Selected Topics in Signal Processing*, *10*(3), 485-500.

[80] Shhab, L. M. H., Rizaner, A., Ulusoy, A. H., & Amca, H. (2017, September). Impact of impulsive noise on millimeter wave cellular systems performance. In *2017 10th UK-Europe-China Workshop on Millimeter Waves and Terahertz Technologies (UCMMT)* (pp. 1-4). IEEE.

[81] Alkhateeb, A., El Ayach, O., Leus, G., & Heath, R. W. (2014). Channel estimation and hybrid precoding for millimeter wave cellular systems. *IEEE Journal of Selected Topics in Signal Processing*, *8*(5), 831-846.

[82] El Ayach, O., Rajagopal, S., Abu-Surra, S., Pi, Z., & Heath, R. W. (2014). Spatially sparse precoding in millimeter wave MIMO systems. *IEEE transactions on wireless communications*, *13*(3), 1499-1513.

[83] T.S. Rappaport, R.W. Heath Jr, R.C. Daniels, J.N. Murdock, *Millimeter wave wireless communications*, Pearson Education, 2014.

[84] Wang, X., & Poor, H. V. (1999). Robust multiuser detection in non-Gaussian channels. *IEEE Transactions on Signal Processing*, *47*(2), 289-305.

[85] Zimmermann, M., & Dostert, K. (2002). Analysis and modeling of impulsive noise in broad-band powerline communications.*IEEE transactions on Electromagnetic compatibility*, *44*(1), 249-258.

[86] Rabie, K. M. (2015). *Power line communication systems* (Doctoral dissertation, University of Manchester). Retrieved from https://www.escholar.manchester.ac.uk/item/?pid=uk-ac-man-scw:282447

[87] Al Mawali, K. (2011). *Techniques for broadband power line communications: impulsive noise mitigation and adaptive modulation* (Doctoral dissertation, RMIT). Retrieved from http://researchbank.rmit.edu.au/view/rmit:13700

[88] Juwono, F. H., Reine, R., Liu, L., Liu, J., & Huang, D. D. (2016, December). Performance of impulsive noise blanking in precoded OFDM-based PLC systems. In *2016 IEEE International Conference on Communication Systems (ICCS)* (pp. 1-6). IEEE.

[89] Rabie, K. M., & Alsusa, E. (2015). Improved DPTE technique for impulsive noise mitigation over power-line communication channels. *AEU-International Journal of Electronics and Communications*, *69*(12), 1847-1853.

[90] Rabie, K. M., & Alsusa, E. (2015, June). Performance analysis of adaptive hybrid nonlinear preprocessors for impulsive noise mitigation over power-line channels. In *2015 IEEE International Conference on Communications (ICC)* (pp. 728-733). IEEE.

[91] Rabie, K. M., Alsusa, E., Familua, A. D., & Cheng, L. (2015, March). Constant envelope OFDM transmission over impulsive noise power-line communication channels. In *2015 IEEE International Symposium on Power Line Communications and Its Applications (ISPLC)* (pp. 13-18). IEEE.

[92] Sarabchi, F., & Nerguizian, C. (2014, September). Impulsive noise mitigation for OFDM-based systems using enhanced blanking nonlinearity. In *2014 IEEE 25th Annual International Symposium on Personal, Indoor, and Mobile Radio Communication (PIMRC)* (pp. 841-845). IEEE.

[93] Hakam, A., Khalid, M., Aly, N. A., Jimaa, S., & Al-Araji, S. (2013, November). MIMO-OFDM system with impulsive noise reduction technique based on auto level Selection Mechanism. In *2013 15th IEEE International Conference on Communication Technology* (pp. 229-233). IEEE.

[94] Epple, U., & Schnell, M. (2016). Advanced blanking nonlinearity for mitigating impulsive interference in OFDM systems. *IEEE Transactions on Vehicular Technology*, *66*(1), 146-158.

[95] Oh, H., & Nam, H. (2016). Design and performance analysis of nonlinearity preprocessors in an impulsive noise environment. *IEEE Transactions on Vehicular Technology*, *66*(1), 364-376.

[96] Ali, Z. (2015, September). Hybrid median-nulling scheme for impulsive noise mitigation in OFDM transmission. In *2015 Fourth International Conference on Aerospace Science and Engineering (ICASE)* (pp. 1-5). IEEE.

[97] Chen, C., & Mow, W. H. (2015, September). Optimized metric clipping decoder design for impulsive noise channels at high signal-to-noise ratios. In *2015 36th IEEE Sarnoff Symposium* (pp. 46-49). IEEE.

[98] Mâad, H. B., Goupil, A., Clavier, L., & Gelle, G. (2010, September). Robust clipping demapper for LDPC decoding in impulsive channel. In *2010 6th International Symposium on Turbo Codes & Iterative Information Processing* (pp. 231-235). IEEE.

[99] Suraweera, H. A., Chai, C., Shentu, J., & Armstrong, J. (2003, September). Analysis of impulse noise mitigation techniques for digital television systems. In 8th Int. OFDM Workshop (pp. 172-176).

[100] Torio, P., & Sánchez, M. G. (2014). Elimination of impulsive noise by double detection in long-term evolution handsets. IEEE Transactions on Vehicular Technology, 64(7), 2875-2882.

[101] Oh, H., & Nam, H. (2016). Design and performance analysis of nonlinearity preprocessors in an impulsive noise environment. IEEE Transactions on Vehicular Technology, 66(1), 364-376.

[102] Zhidkov, S. V. (2008). Analysis and comparison of several simple impulsive noise mitigation schemes for OFDM receivers. IEEE Transactions on Communications, 56(1), 5-9.

[103] Zhidkov, S. V. (2006). Performance analysis and optimization of OFDM receiver with blanking nonlinearity in impulsive noise environment. IEEE transactions on vehicular technology, 55(1), 234-242.

[104] Banelli, P. (2013). Bayesian estimation of a Gaussian source in Middleton's class-A impulsive noise. IEEE Signal Processing Letters, 20(10), 956-959.

[105] Darsena, D., Gelli, G., Melito, F., & Verde, F. (2015). ICI-free equalization in OFDM systems with blanking preprocessing at the receiver for impulsive noise mitigation. IEEE Signal Processing Letters, 22(9), 1321-1325.

[107] Rugini, L., & Banelli, P. (2016). On the equivalence of maximum SNR and MMSE estimation: applications to additive non-Gaussian channels and quantized observations. IEEE Transactions on Signal Processing, 64(23), 6190-6199.

[108] Vastola, K. (1984). Threshold detection in narrow-band non-Gaussian noise. IEEE Transactions on Communications, 32(2), 134-139.

[109] Caspers, F. (2012). RF measurements I: signal receiving techniques. arXiv preprint arXiv:1201.3247.

[110] Koch, W. R. (1939). U.S. Patent No. 2,166,995. Washington, DC: U.S. Patent and Trademark Office.

[111] Trousdale, R. B. (1954). U.S. Patent No. 2,676,250. Washington, DC: U.S. Patent and Trademark Office.

[112] Broadhead, J. S. L., & Schoenike, E. O. (1962). U.S. Patent No. 3,056,087. Washington, DC: U.S. Patent and Trademark Office.